1-1-2007

Performance analysis of OFDM-ROF system

Deepak C. Isac
Ryerson University

Performance Analysis of OFDM-ROF System

By

Deepak C Isac

A Project Report

Presented to Ryerson University

in partial fulfillment of the requirements for the degree of

Master of Engineering

in the department of

Electrical and Computer Engineering

RYERSON UNIVERSITY

TORONTO CANADA, 2007

Dedicated to

Late Rev.Fr.Philiph Chackalamuriyil

Access to Project

I, the undersigned, the author of this project, understand that Ryerson University will make it available for use within the University Library and, by microfilm or other photographic means, allow access to users in other approved libraries. All users consulting this project will have to sign the following statement:

"In consulting this project I agree not to copy or closely paraphrase it in whole or in part without the written consent of the author; and to make proper written acknowledgement for any assistance which I have obtained from it."

Beyond this, I do not wish to place any restriction on access to this project

....

(signature) (date)

Declaration

I declare that this project is my own work and has not been submitted in any form for another degree or diploma at any university or other institution of tertiary education. Information derived from the published work of others has been acknowledged in the text and a list of references is given.

(Deepak C Isac)

Acknowledgements

I wish to convey warmest thanks to my parents, who have given me endless support.

I wish to thank my supervisor Prof Xavier Fernando for his extreme help, support and encouragement.

I also thank Prof Alagan Anpalagan, Director, Graduate studies, Department of Electrical and Computer Engineering, Ryerson University for his expert help and recommendations.

I would also like to thank Julie and Delvin for their inspiration support and for sharing my excitement of discoveries made during this project

I would like to thank Jobin and Aneesh for the many hours of white board discussion.

I would particularly like to thank Dr.D.S.Pundhir, Dr. C. K. Singh and Dr.S.A.M Rizvi for their motivational discussions about research and publications

I also would like to thank all staff of the School of Engineering at Ryerson University for their kind help.

ABSTRACT

The demand for high-speed mobile wireless communications is rapidly growing. Orthogonal Frequency Division Multiplexing (OFDM) technology promises to be a key technique for achieving the high data capacity and spectral efficiency requirements for wireless communication systems of the near future. The practical results will be more yielding when the OFDM is combined with Radio Over Fiber technology (ROF). This project presents an investigation on the performance of OFDM-ROF system based on papers [95] [96] [97] [98] in terms of peak power reduction capability, degradation of channel capacity. OFDM is an attractive technique for achieving high-bit-rate wireless data transmission. However, the potentially large peak-to-average power ratio *(PAPR)* of a multicarrier signal has limited its application. The analysis is based on three sections 1.Peak to average power Ratio 2. Signal distortion and channel capacity 3. ROF transmission. This project report is organized as follows. After the introduction in second chapter OFDM and its principles are studied. Thirdly, a throughput on the basic ROF technology .The fourth chapter is based on OFDM-ROF system, its basic model and description. Fifth chapter is PAPR and instantaneous power analysis. The effect of the envelope clipping on the peak-to-average power ratio (PAPR) and then instantaneous power of the band-limited OFDM signal is studied. While doing the PAPR analysis, the different approaches for the reduction of PAPR by different authors are compared. The sixth chapter is regarding the Signal distortion and channel capacity over additive white Gaussian noise and Rayleigh fading channels. The capacity calculations shown are based on the assumption that the distortion terms caused by the clipping are Gaussian .In seventh chapter the ROF transmission analysis is based on split-step Fourier method and nonlinear Schrödinger equation. The transmission performance is discussed from the measurement values by incorporating the spectral distribution of a modulation signal into the calculation of composite triple beats. Also presented the dynamic range of OFDM-64QAM which is evaluated from the calculations of Desired to Undesired Signal Ratio (DUR).Thus this project evaluates the OFDM-ROF system as a candidate for the future (4G) wireless system design.

TABLE OF CONTENTS

GLOSSARY

2G	-	Second Generation mobile phone system (GSM, IS-95)
3G	-	Third Generation mobile phone system (systems using WCDMA)
4G	-	Fourth Generation mobile phone system
alpha	-	Path loss exponent (rate of path loss change with distance)
ASK	-	Amplitude Shift Keying
AWGN	-	Additive White Gaussian Noise
b/s/Hz	-	Bits per second per hertz (unit of spectral efficiency)
BER	-	Bit Error Rate
bps	-	Bits per second
BPSK	-	Binary Phase Shift Keying
BS	-	Base Station
CD	-	Compact Disc
CDMA	-	Code Division Multiple Access
CF	-	Crest Factor (peak to average power ratio of the RF envelope)
DAB	-	Digital Audio Broadcasting
dB	-	Decibel (ratio in log scale)
dBc	-	Decibel relative to main signal power sir
dBm	-	Decibel relative to 1 milliwatt
DC	-	Direct Current (0 Hz)
DDS	-	Direct Digital Synprojecter
DFT	-	Discrete Fourier Transform
DMT	-	Discrete Multi-Tone
DPSK	-	Differential Phase Shift Keying
DSBSC	-	Double Side Band Suppressed Carrier
DS-CDMA	-	Direct Sequence Code Division Multiple Access
DSP	-	Digital Signal Processing
DSSS	-	Direct Sequence Spread Spectrum
DVB	-	Digital Video Broadcasting
DVB-C	-	Digital Video Broadcasting – Cable
DVB-S	-	Digital Video Broadcasting – Satellite
DVB-T	-	Digital Video Broadcasting - Terrestrial

EBNR	-	Energy per Bit to Noise Ratio
FDM	-	Frequency Division Multiplexing
FEC	-	Forward Error Correction
FFT	-	Fast Fourier Transform
FIR	-	Finite Impulse Response (digital filter)
FM	-	Frequency Modulation
Fs	-	Sample Frequency
FSK	-	Frequency Shift Keying
GA	-	Genetic Algorithm
GHz	-	Gigahertz - 10_9 Hz
GMSK	-	Gaussian Minimum Shift Keying
GSM	-	Global System for Mobile communications
HDTV	-	High Definition Television
HiperLAN2	-	High Performance Radio Local Area Network, WLAN standard (Europe) based on OFDM, with a maximum data rate of 54 Mbps. Similar to IEEE802.11a
Hz	-	Hertz (cycles per second)
ICI	-	Inter-Carrier Interference
IEEE802.11a	-	WLAN standard (U.S.) based on OFDM, with a maximum data rate of 54 Mbps. Similar to HiperLAN2
IEEE802.11b	-	WLAN standard (U.S.) based on DSSS, with a maximum data rate of 11 Mbps
IF	-	Intermediate Frequency
IFFT	-	Inverse Fast Fourier Transform
IMD	-	Inter-Modulation Distortion
IQ	-	Inphase Quadrature
ISI	-	Inter-Symbol Interference
ISM	-	Industrial Scientific Medical
IS-95	-	Mobile phone standard using CDMA transmission method.
JCU	-	James Cook University
K	-	Kelvin
kbps	-	Kilo bits per second (10_3 bps)
kHz	-	Kilohertz - 10_3 Hz
km	-	Kilometer (10_3 m)
l	-	Lambda - RF wavelength
LO	-	Local Oscillator

LOS	-	Line Of Sight
m	-	Meter
Mbps	-	Mega bits per second (10^6 bps)
MHz	-	Megahertz - 10^6Hz
MPEG	-	Moving Picture Experts Group (Video compression standard)
NF	-	Receiver Noise Figure
OBO	-	Output power Back Off
OFDM	-	Orthogonal Frequency Division Multiplexing
PAPR	-	Peak to Average Power Ratio
PM	-	Phase Modulation
PRC	-	Peak Reduction Carriers
PRS	-	Pseudo Random Sequence
PSK	-	Phase Shift Keying
QAM	-	Quadrature Amplitude Modulation
QOS	-	Quality Of Service
QPSK	-	Quadrature Phase Shift Keying
RF	-	Radio Frequency
RMS	-	Root Mean Squared
SFN	-	Single Frequency Network
SHARC	-	Super Harvard Architecture, Digital Signal Processor by Analog Devices)
SIR	-	Signal to Interference Ratio
SNR	-	Signal to Noise Ratio
SSB	-	Single Side Band
SSPA	-	Solid State Power Amplifier
TDM	-	Time Division Multiplexing
TDMA	-	Time Division Multiple Access
TWTA	-	Traveling Wave Tube Amplifier
Mm	-	Micrometer (10^{-6} m)
UMTS	-	Universal Mobile Telecommunications System
ms	-	Microsecond (10^{-6} s)
W	-	Watt (energy per unit time, one joule per second)
W-CDMA	-	Wide-band Code Division Multiple Access
WLAN	-	Wireless Local Area Network
WLL	-	Wireless Local Loop

1. INTRODUCTION

During the last several years, wireless communication has not only created new businesses, but also made a great change in our life style. Second generation (2G) mobile communication systems based on digital signal processing techniques has been very successful for decades. It leads to the development of third generation mobile systems. Third generation (3G) mobile communication systems, wideband code-division multiple access (WCDMA), and CDMA2000, it is better to be high performance and high bandwidth systems to carry high data rate services. During the evolution from 2G to 3G, a variety of wireless systems such as GPRS, Bluetooth, UWB, Wireless LAN (WLAN), and HiperLAN, have been developed. These systems are designed independently, with an aim of different service types, data rates, and users. Because these systems all have their own merits and shortcomings, there will be no single system that is good enough to replace all the other technologies.

Nowadays, researchers, system vendors, and service providers are expressing growing interest in future wireless communication systems that can support various service types and various users demand. The important features of future wireless communication systems are following: *Ubiquitous*; anywhere, anytime, with any device *Broadband*: sufficient data rate to deliver various services *Convergence*: support of various service types, data rates and users. *Seamless*: always best connected, global roaming across multiple wireless and mobile networks.

Wireless communications is an emerging field, which has seen enormous growth in the last several years. The huge uptake rate of mobile phone technology, Wireless Local Area Networks (WLAN) and the exponential growth of the Internet have resulted in an increased demand for new methods of obtaining high capacity wireless networks. Most WLAN systems currently use the IEEE802.11b standard, which provides a maximum data rate of 11 Mbps [36]. WLAN standards such as IEEE802.11a [40] and HiperLAN2 [38], [39] are based on OFDM technology and provide a much higher data rate of 54 Mbps. However systems of the near future will require WLANs with data rates of greater than 100 Mbps, and so there is a need to further improve the spectral efficiency and data capacity of OFDM systems in WLAN applications. For cellular mobile applications, we will see in the near future a

complete convergence of mobile phone technology, computing, Internet access, and potentially many multimedia applications such as video and high quality audio. In fact, some may argue that this convergence has already largely occurred, with the advent of being able to send and receive data using a notebook computer and a mobile phone. Although this is possible with current 2G (2nd Generation) Mobile phones, the data rates provided are very low (9.6 kbps – 14.4 kbps) and the cost is high (typically $0.15 - $1.25 per minute) [24], [25], limiting the usefulness of such a service. The goal of third and fourth generation mobile networks is to provide users with a high data rate, and to provide a wider range of services, such as voice communications, videophones, and high speed Internet access. The higher data rate of future mobile networks will be achieved by increasing the amount of spectrum allocated to the service and by improvements in the spectral efficiency. OFDM is a potential candidate for the physical layer of fourth generation mobile systems. This project presents performance analysis of OFDM-ROF system.

1.1 Third Generation (current) wireless systems

Third generation mobile systems such as the Universal Mobile Telecommunications System (UMTS) [1], [2], [3], [4] and CDMA2000 [6] are introduced over the last years (2002 onwards) [5]. Third generation systems use WCDMA as the carrier modulation scheme [10]. This modulation scheme has a high multipath tolerance, flexible data rate, and allows a greater cellular spectral efficiency than 2G systems. Third generation systems will provide a significantly higher data rate (64 kbps – 2 Mbps) [1] than second-generation systems (9.6 – 14.4 kbps). The higher data rate of 3G systems will be able to support a wide range of applications including Internet access, voice communications and mobile videophones. In addition to this, a large number of new applications will emerge to utilize the permanent network connectivity, such as wireless appliances, notebooks with built in mobile phones, remote logging, wireless web cameras, car navigation systems, and so forth. In fact most of these applications will not be limited by the data rate provided by 3G systems, but by the cost of the service. The demand for use of the radio spectrum is very high, with terrestrial mobile phone systems being just one of many applications varying for suitable bandwidth. These applications require the system to operate reliably in non-line-of-sight environments with a propagation distance of 0.5 - 30 km, and at velocities up to 100 km/hr or higher. This operating environment limits the maximum RF frequency to 5 GHz, as operating above this

frequency results in excessive channel path loss, and excessive Doppler spread at high velocity. This limits the spectrum available for mobile applications, making the value of the radio spectrum extremely high. In Europe auctions of 3G licenses of the radio spectrum began in 1999. In the United Kingdom, 90 MHz of bandwidth [8] was auctioned off for £22.5 billion [9]. In Germany the result was similar, with 100 MHz of bandwidth raising $46 billion (US) [7]. This represents a value of around $450 Million (US) per MHz. The length of these license agreements is 20 years [8] and so to obtain a reasonable rate of return of 8% on investment, $105 Million (US) per MHz must be raised per year. It is therefore vitally important that the spectral efficiency of the communication system is maximized, as this is one of the main limitations in providing a low cost high data rate service.

1.2 Future Generation (4G) systems

Research has just recently begun on the development of 4th generation (4G) mobile communication systems. The commercial rollout of these systems is likely to begin around 2008 - 2012, and will replace 3rd generation technology. Ultimately 4G networks should encompass broadband wireless services, such as High Definition Television (HDTV) (4 - 20 Mbps) and computer network applications (1 - 100 Mbps). This will allow 4G networks to replace many of the functions of WLAN systems. However, to cover this application, cost of service must be reduced significantly from 3G networks. The spectral efficiency of 3G networks is too low to support high data rate services at low cost. As a consequence one of the main focuses of 4G systems will be to significantly improve the spectral efficiency. In addition to high data rates, future systems must support a higher Quality Of Service (QOS) than current cellular systems, which are designed to achieve 90 - 95% coverage [11], i.e. network connection can be obtained over 90 - 95% of the area of the cell. This will become inadequate as more systems become dependent on wireless networking. As a result 4G systems are likely to require a QOS closer to 98 ├ 99.5%. In order to achieve this level of QOS it will require the communication system to be more flexible and adaptive. In many applications it is more important to maintain network connectivity than the actual data rate achieved. If the transmission path is very poor, e.g. in a building basement, then the data rate has to drop to maintain the link. Thus the data rate might vary from as low as 1 kbps in extreme conditions, to as high as 20 Mbps for a good transmission path.

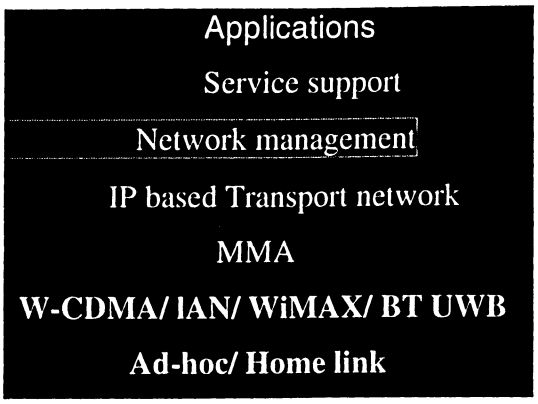

Fig.1.1 4G Architecture

Alternatively, for applications requiring the QOS can be improved by allocating additional resources to users with a poor transmission path. A significant improvement in nonlinearity effects will be required in order for 4G systems to provide true broadband access. This will only be achieved by significant advances in multiple aspects of cellular network systems, such as network structure, network management, smart antennas, RF modulation, user allocation, and general resource allocation. This project will focus on the aspects of PAPR issues and method of reduction, signal distortion, channel capacity and RoF transmission issues.

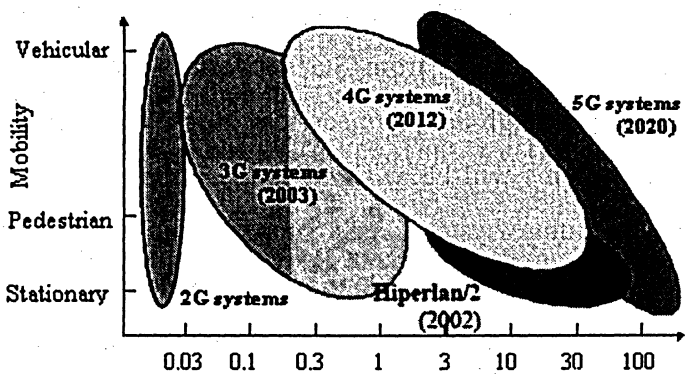

Fig.1.2.Wirlesss Generation systems[2]

1.3 Digital Audio and Video Broadcasting (DAB and DVB)

DAB was the first commercial use of OFDM technology [19], [20]. Development of DAB started in 1987 and services began in U.K and Sweden in 1995. DAB is a replacement for

FM audio broadcasting, by providing high quality digital audio and information services. OFDM was used for DAB due to its multipath tolerance. Broadcast systems operate with potentially very long transmission distances (20 - 100 km). As a result, multipath is a major problem as it causes extensive ghosting of the transmission. This ghosting causes Inter-Symbol Interference (ISI), blurring the time domain signal. For single carrier transmissions the effects of ISI are normally mitigated using adaptive equalization. This process uses adaptive filtering to approximate the impulse response of the radio channel. An inverse channel response filter is then used to recombine the blurred copies of the symbol bits. This process is however complex and slow due to the locking time of the adaptive equalizer. Additionally it becomes increasing difficult to equalize signals that suffer ISI of more than a couple of symbol periods. OFDM overcomes the effects of multipath by breaking the signal into many narrow bandwidth carriers. This results in a low symbol rate reducing the amount of ISI. In addition to this, a guard period is added to the start of each symbol, removing the effects of ISI for multipath signals delayed less than the guard period. The high tolerance to multipath makes OFDM more suited to high data transmissions in terrestrial environments than single carrier transmissions.

Transmission Mode Parameters

Parameter	**Transmission Mode**			
	I	**II**	**III**	**IV**
Bandwidth	1.536 MHz	1.536 MHz	1.536 MHz	1.536 MHz
Modulation	DQPSK	DQPSK	DQPSK	DQPSK
Frequency Range (Mobile reception)	≤375 MHz	≤1.5 GHz	≤3 GHz	≤1.5 GHz
Number of subcarriers	1536	384	192	768
Symbol Duration	1000 μs	250 μs	125μs	500 μs
Guard Duration	246 μs	62 μs	31 μs	123 μs
Total Symbol Duration	1246 μs	312 μs	156 μs	623μs
Maximum Transmitter Separation for SFN	96 km	24 km	12 km	48 km

Table 1-1: system parameters for DAB.

DAB has four transmission modes. The transmission frequency, receiver velocity and required multipath tolerance all determine the most suitable transmission mode to use. Doppler spread is caused by rapid changes in the channel response due to movement of the receiver through a multipath environment. It results in random frequency modulation of the OFDM subcarriers, leading to signal degradation. The amount of Doppler spread is proportional to the transmission frequency and the velocity of movement. The closer the subcarriers are spaced together, the more susceptible the OFDM signal is to Doppler spread, and so the different transmission modes in DAB allow trade off between the amount of multipath protection (length of the guard period) and the Doppler spread tolerance. The high multipath tolerance of OFDM allows the use of a Single Frequency Network (SFN), which uses transmission repeaters to provide improved coverage, and spectral efficiency. For traditional FM broadcasting, neighboring cities must use different RF frequencies even for the same radio station, to prevent multipath causes by rebroadcasting at the same frequency. However, with DAB it is possible for the same signal to be broadcast from every area requiring coverage, eliminating the need for different frequencies to be used in neighboring areas. The data throughput of DAB varies from 0.6 - 1.8 Mbps depending on the amount of Forward Error Correction (FEC) applied. This data payload allows multiple channels to be broadcast as part of the one transmission ensemble. The number of audio channels is variable depending on the quality of the audio and the amount of FEC used to protect the signal. For telephone quality audio (24 kbps) up to 64 audio channels can be provided, while for CD quality audio (256 kb/s), with maximum protection, three channels are available. More information on DAB can be found in [20] and [21].

The development of the Digital Video Broadcasting (DVB) standards was started in 1993 [14]. DVB is a transmission scheme based on the MPEG-2 standard, as a method for point to multipoint delivery of high quality compressed digital audio and video. It is an enhanced replacement of the analogue television broadcast standard, as DVB provides a flexible transmission medium for delivery of video, audio and data services [17]. The DVB standards specify the delivery mechanism for a wide range of applications, including satellite TV (DVB-S), cable systems (DVB-C) and terrestrial transmissions (DVB-T) [15]. The physical layer of each of these standards is optimized for the transmission channel being used. Satellite broadcasts use a single carrier transmission, with QPSK modulation, which is

optimized for this application as a single carrier allows for large Doppler shifts, and QPSK allows for maximum energy efficiency [16]. This transmission method is however unsuitable for terrestrial transmissions as multipath severely degrades the performance of high-speed single carrier transmissions. For this reason, OFDM was used for the terrestrial transmission standard for DVB. The physical layer of the DVB-T transmission is similar to DAB, in that the OFDM transmission uses a large number of subcarriers to mitigate the effects of multipath. DVB-T allows for two transmission modes depending on the number of subcarriers used [18]. Table 1-2 shows the basic transmission parameters for these two modes.

The major difference between DAB and DVB-T is the larger bandwidth used and the use of higher modulation schemes to achieve a higher data throughput. The DVB-T allows for three subcarrier modulation schemes: QPSK, 16-QAM (Quadrature Amplitude Modulation) and 64- QAM; and a range of guard period lengths and coding rates. This allows the robustness of the transmission link to be traded at the expense of link capacity... DVB-T is a uni-directional link due to its broadcast nature. Thus any choice in data rate verses robustness affects all receivers. If the system goal is to achieve high reliability, the data rate must be low; it is ready to meet the conditions of the worst receiver. This effect limits the usefulness of the flexible nature of the standard. However if these same principles of a flexible transmission rate are used in bi-directional communications, the data rate can be maximized based on the current radio conditions. Additionally for multiuser applications, it can be optimized for individual remote transceivers.

1.4 Hiperlan2 and IEEE802.11A

Development of the European Hiperlan standard was started in 1995, with the final standard of HiperLAN2 being defined in June 1999. HiperLAN2 pushes the performance of WLAN systems, allowing a data rate of up to 54 Mbps [37]. HiperLAN2 uses 48 data and 4 pilot subcarriers in a 16 MHz channel, with 2 MHz on either side of the signal to allow out of band roll off. User allocation is achieved by using TDM, and subcarriers are allocated using a range of modulation schemes, from BPSK up to 64-QAM, depending on the link quality. Forward Error Correction is used to compensate for frequency selective fading. IEEE802.11a has the same physical layer as HiperLAN2 with the main difference between the standard

corresponding to the higher-level network protocols used. HiperLAN2 is used extensively as an example OFDM system in this project. Since the physical layer of HiperLAN2 is very similar to the IEEE802.11a standard these examples are applicable to both standards

Standard	802.11b	802.11a	HiperLAN2
Spectrum	2.4 GHz	5.2 GHz	5.2 GHz
Modulation Technique	DSSS	OFDM	OFDM
~Max physical rate	11Mbps	54 Mbps	54 Mpbs
~Max data rate, layer 3	5Mbps	32 Mbps	32 Mpbs
Medium access control	CSMA/CA		TDMA/TDD
Connectivity	Conn.less	Conn. Less	Conn. Oriented

Table 1-2, Summary of characteristics of IEEE802.11b, IEEE802.11a and HiperLAN2. Derived from [37]

Parameter	Value
Channel Spacing	20 MHz
IFFT used for 20 MSPS	64
Data Subcarriers	48
Pilot Subcarriers	4
Carrier Spacing (F_c)	312.5 kHz (=20 MHz/64)
Nominal Bandwidth	16.25 MHz (=312.5 kHz x 52)
Useful Symbol Period	3.2 µsec (=1/F_C)
Guard Period	0.8 µsec
Modulation Schemes	BPSK, QPSK, 16-QAM, 64-QAM
Coding Rate	½, 2/3, ¾

Table 1-3, Physical Layer for HiperLAN2 and IEEE802.11a. Derived from [39]

2. ORTHOGONAL FREQUENCY DIVISION MULTIPLEXING (OFDM)

Orthogonal Frequency Division Multiplexing (OFDM) is an alternative wireless modulation technology to CDMA. OFDM has the potential to surpass the capacity of CDMA systems and provide the wireless access method for 4G systems. OFDM is a modulation scheme that allows digital data to be efficiently and reliably transmitted over a radio channel, even in multipath environments. OFDM transmits data by using a large number of narrow bandwidth carriers. These carriers are regularly spaced in frequency, forming a block of spectrum. The frequency spacing and time synchronization of the carriers is chosen in such a way that the carriers are orthogonal, meaning that they do not cause interference to each other. This is despite the carriers overlapping each other in the frequency domain. The name 'OFDM' is derived from the fact that the digital data is sent using many carriers, each of a different frequency (Frequency Division Multiplexing) and these carriers are orthogonal to each other, hence Orthogonal Frequency Division Multiplexing. The origins of OFDM development started in the late 1950's [30] with the introduction of Frequency Division Multiplexing (FDM) for data communications. In 1966 Chang patented the structure of OFDM [32] and published [31] the concept of using orthogonal overlapping multi-tone signals for data communications. In 1971 the it is [33] introduced the idea of using a Discrete Fourier Transform (DFT) for implementation of the generation and reception of OFDM signals, eliminating the requirement for banks of analog subcarrier oscillators. This presented an opportunity for an easy implementation of OFDM, especially with the use of Fast Fourier Transforms (FFT), which are an efficient implementation of the DFT. This suggested that the easiest implementation of OFDM is with the use of Digital Signal Processing (DSP), which can implement FFT algorithms. It is only recently that the advances in integrated circuit technology have made the implementation of OFDM cost effective. The reliance on DSP prevented the wide spread use of OFDM during the early development of OFDM. It wasn't until the late 1980's that work began on the development of OFDM for commercial use, with the introduction of the Digital Audio Broadcasting (DAB) system.

2.1 Principles of OFDM

Orthogonal Frequency Division Multiplexing (OFDM) is very similar to the well-known and used technique of Frequency Division Multiplexing (FDM). OFDM uses the principles of FDM to allow multiple messages to be sent over a single radio channel. It is however in a much more controlled manner, allowing an improved spectral efficiency.

A simple example of FDM is the use of different frequencies for each FM (Frequency Modulation) radio stations. All stations transmit at the same time but do not interfere with each other because they transmit using different carrier frequencies. Additionally they are bandwidth limited and are spaced sufficiently far apart in frequency so that their transmitted signals do not overlap in the frequency domain. At the receiver, each signal is individually received by using a frequency tunable band pass filter to selectively remove all the signals except for the station of interest. This filtered signal can then be demodulated to recover the original transmitted information.

OFDM is different from FDM in several ways. In conventional broadcasting each radio station transmits on a different frequency, effectively using FDM to maintain a separation between the stations. There is however no coordination or synchronization between each of these stations. With an OFDM transmission such as DAB, the information signals from multiple stations are combined into a single multiplexed stream of data. This data is then transmitted using an OFDM ensemble that is made up from a dense packing of many subcarriers. All the subcarriers within the OFDM signal are time and frequency synchronized to each other, allowing the interference between subcarriers to be carefully controlled. These multiple subcarriers overlap in the frequency domain, but do not cause Inter-Carrier Interference (ICI) due to the orthogonal nature of the modulation. Typically with FDM the transmission signals need to have a large frequency guard-band between channels to prevent interference. This is the overall spectral efficiency. However with OFDM the orthogonal packing of the subcarriers greatly reduces this guard band, improving the spectral efficiency.

All wireless communication systems use a modulation scheme to map the information signal to a form that can be effectively transmitted over the communications channel. A wide range of modulation schemes has been developed, with the most suitable one, depending on whether the information signal is an analogue waveform or a digital signal. Some of the

common analogue modulation schemes include Frequency Modulation (FM), Amplitude Modulation (AM), Phase Modulation (PM), Single Side Band (SSB), Vestigial Side Band (VSB), Double Side Band Suppressed Carrier (DSBSC) [41], [42]. Common single carrier modulation schemes for digital communications include Amplitude Shift Keying (ASK), Frequency Shift Keying (FSK), Phase Shift Keying (PSK) and Quadrature Amplitude Modulation (QAM) [41] - [43].

Each of the carriers in a FDM transmission can use an analogue or digital modulation scheme. There is no synchronization between the transmission and so one station could transmit using FM and another in digital using FSK. In a single OFDM transmission all the subcarriers are synchronized to each other, restricting the transmission to digital modulation schemes. OFDM is symbol based, and can be thought of as a large number of low bit rate carriers transmitting in parallel. All these carriers transmit in unison using synchronized time and frequency, forming a single block of spectrum. This is to ensure that the orthogonal nature of the structure is maintained. Since these multiple carriers form a single OFDM transmission, they are commonly referred to as 'subcarriers', with the term of 'carrier' reserved for describing the RF carrier mixing the signal from base band.

2.1.1 Orthogonality

Signals are orthogonal if they are mutually independent of each other. Orthogonality is a property that allows multiple information signals to be transmitted perfectly over a common channel and detected, without interference. Loss of orthogonality results in blurring between these information signals and degradation in communications. In the frequency domain most FDM systems are orthogonal as each of the separate transmission signals are It is all spaced out in frequency preventing interference. Although these methods are orthogonal the term OFDM has been reserved for a special form of FDM. The subcarriers in an OFDM signal are spaced as close as is theoretically possible while maintain orthogonality between them.

OFDM achieves orthogonality in the frequency domain by allocating each of the separate information signals onto different subcarriers. OFDM signals are made up from a sum of sinusoids, with each corresponding to a subcarrier. The baseband frequency of each subcarrier is chosen to be an integer multiple of the inverse of the symbol time, resulting in all subcarriers having an integer number of cycles per symbol. As a consequence the

subcarriers are orthogonal to each other. Figure 2-1 below shows the construction of an OFDM signal with four subcarriers

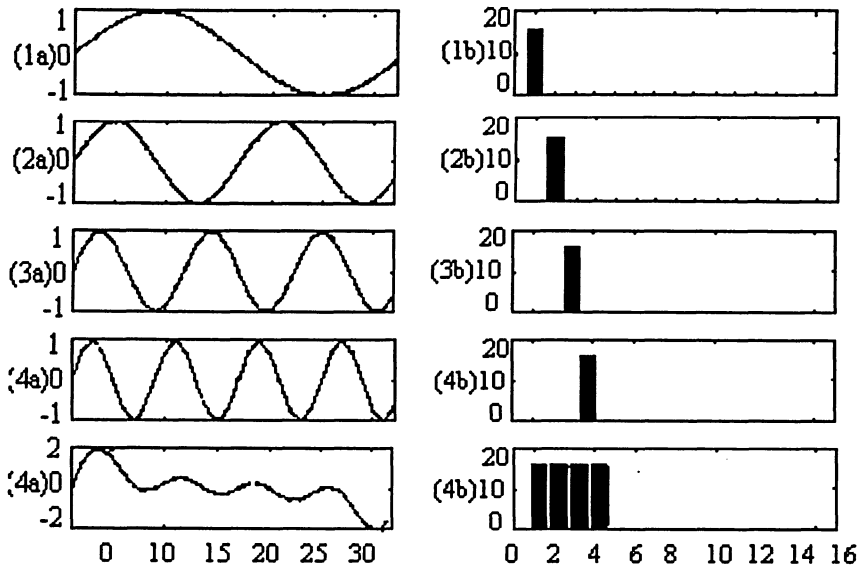

Figure 2-1, Time domain construction of an OFDM signal. (1a), (2a), (3a) and (4a) show individual subcarriers, with 1, 2, 3, and 4 cycles per symbol respectively. The phase on all these subcarriers is zero. Note, that each subcarrier has an integer number of cycles per symbol, making them cyclic. Adding a copy of the symbol to the end would result in a smooth join between symbols. (1b), (2b), (3b) and (4b) show the FFT of the time waveforms in (1a), (2a), and (3a) and (4a) respectively. (4a) and (4b) shows the result for the summation of the 4 subcarriers.

Sets of functions are orthogonal to each other if they match the conditions in equation (2-1). If any two different functions within the set are multiplied, and integrated over a symbol period, the result is zero, for orthogonal functions. Another way of thinking of this is that, if we look at a matched receiver for one of the orthogonal functions, a subcarrier in the case of OFDM, then the receiver will only see the result for that function. The results from all other functions in the set integrate to zero, and thus have no effect.

$$\int_0^T s_i(t)s_j(t)dt = \begin{cases} C & i = j \\ O & i \neq j \end{cases} \qquad (2\text{-}1)$$

Equation (2-2) shows a set of orthogonal sinusoids, which represent the subcarriers for an unmodulated real OFDM signal.

$$s_k(t) = \begin{cases} \sin(2\pi k f_0 t) & 0 < t < T \quad k = 1,2,\ldots M \\ 0 & otherwise \end{cases} \qquad (2\text{-}2)$$

where f_o is the carrier spacing, M is the number of carriers, T is the symbol period. Since the highest frequency component is *Mfo* the transmission bandwidth is also *Mfo* .

These subcarriers are orthogonal to each other because when we multiply the waveforms of any two subcarriers and integrate over the symbol period the result is zero. Multiplying the two sine waves together is the same as mixing these subcarriers. This results in sum and difference frequency components, which will always be integer subcarrier frequencies, as the frequency of the two mixing subcarriers has integer number of cycles. Since the system is linear, we can integrate the result by taking the integral of each frequency component separately then combining the results by adding the two sub-integrals. The two frequency components after the mixing have an integer number of cycles over the period and so the sub-integral of each component will be zero, as the integral of a sinusoid over an entire period is zero. Both the sub-integrals are zeros and so the resulting addition of the two will also be zero, thus it is established that the frequency components are orthogonal to each other.

2.1.2 Frequency Domain Orthogonality

Another way to view the orthogonality property of OFDM signals is to look at its spectrum. In the frequency domain each OFDM subcarrier has a sinc, *sin(x)/x,* frequency response, as shown in Figure 2-2. This is a result of the symbol time corresponding to the inverse of the carrier spacing. As far as the receiver is concerned each OFDM symbol transmitted for a fixed time (T_{FFT}) with no tapering at the ends of the symbol. This symbol time corresponds to the inverse of the subcarrier spacing of $1/T_{FFT}$ Hz. This rectangular waveform in the time domain results in a *sinc* frequency response in the frequency domain. The *sinc* shape has a narrow main lobe, with many side-lobes that decay slowly with the magnitude of the frequency difference away from the centre. Each carrier has a peak at the centre frequency and nulls evenly spaced with a frequency gap equal to the carrier spacing.

The orthogonal nature of the transmission is a result of the peak of each subcarrier corresponding to the nulls of all other subcarriers. When this signal is detected using a Discrete Fourier Transform (DFT) the spectrum is not continuous as shown in Figure 2-2 (a), but has discrete samples. The sampled spectrum is shown as 'o's in the figure. If the DFT is time synchronized, the frequency samples of the DFT correspond to just the peaks of the

subcarriers, thus the overlapping frequency region between subcarriers does not affect the receiver. The measured peaks correspond to the nulls for all other subcarriers, resulting in orthogonality between the subcarriers.

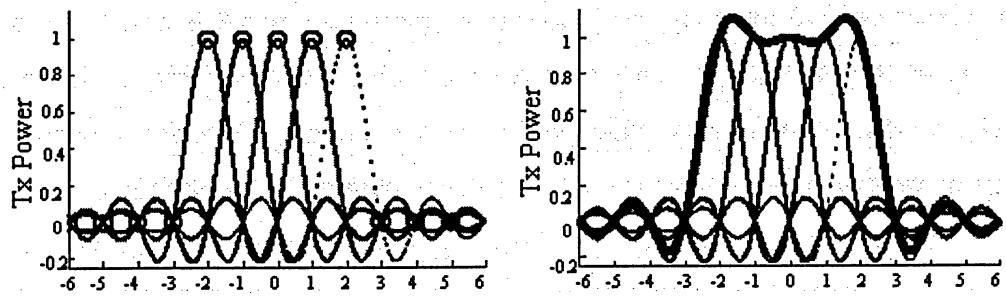

Figure 2-2, Frequency response of the subcarriers in a 5 tone OFDM signal.

(a) Shows the spectrum of each carrier, and the discrete frequency samples seen by an OFDM receiver. Note, each carrier is sinc, $sin(x)/x$, in shape. (b) Shows the overall combined response of the 5 subcarriers (thick black line).

2.2 OFDM Generation and Reception

OFDM signals are typically generated digitally due to the difficulty in creating large banks of phase lock oscillators and receivers in the analog domain. The transmitter section converts digital data to be transmitted, into a mapping of subcarrier amplitude and phase. It then transforms this spectral representation of the data into the time domain using an Inverse Discrete Fourier Transform (IDFT). The Inverse Fast Fourier Transform (IFFT) performs the same operations as an IDFT, except that it is much more computationally efficiency, and so is used in all practical systems. In order to transmit the OFDM signal the calculated time domain signal is then mixed up to the required frequency. The receiver performs the reverse operation of the transmitter, mixing the RF signal to base band for processing, then using a Fast Fourier Transform (FFT) to analyze the signal in the frequency domain. The amplitude and phase of the subcarriers is then picked out and converted back to digital data. The IFFT and the FFT are complementary function and the most appropriate term depends on whether the signal is being received or generated. In cases where the signal is independent of this distinction then the term FFT and IFFT is used interchangeably.

2.2.1 Serial to Parallel Conversion

Data to be transmitted is typically in the form of a serial data stream. In OFDM, each symbol typically transmits 40 - 4000 bits, and so a serial to parallel conversion stage is needed to convert the input serial bit stream to the data to be transmitted in each OFDM symbol. The data allocated to each symbol depends on the modulation scheme used and the number of subcarriers. For example, for a subcarrier modulation of 16-QAM each subcarrier carries 4 bits of data, and so for a transmission using 100 subcarriers the number of bits per symbol would be 400.

For adaptive modulation schemes, the modulation scheme used on each subcarrier can vary and so the number of bits per subcarrier also varies. As a result the serial to parallel conversion stage involves filling the data payload for each subcarrier. At the receiver the reverse process takes place, with the data from the subcarriers being converted back to the original serial data stream.

When an OFDM transmission occurs in a multipath radio environment, frequency selective fading can result in groups of subcarriers being heavily attenuated, which in turn can result in bit errors. These nulls in the frequency response of the channel can cause the information sent in neighbouring carriers to be destroyed, resulting in a clustering of the bit errors in each symbol. Most Forward Error Correction (FEC) schemes tend to work more effectively if the errors are spread evenly, rather than in large clusters, and so to improve the performance most systems employ data scrambling as part of the serial to parallel conversion stage. This is implemented by randomizing the subcarrier allocation of each sequential data bit. At the receiver the reverse scrambling is used to decode the signal. This restores the original sequencing of the data bits, but spreads clusters of bit errors so that they are approximately uniformly distributed in time. This randomization of the location of the bit errors improves the performance of the FEC and the system as a whole.

2.2.2 Subcarrier Modulation

Once each subcarrier has been allocated bits for transmission, they are mapped using a modulation scheme to a subcarrier amplitude and phase, which is represented by a complex In-phase and Quadrature-phase (IQ) vector3. In 16-QAM, which maps 4 bits for each symbol, each combination of the 4 bits of data corresponds to a unique IQ vector, shown as a

dot on the figure. A large number of modulation schemes are available allowing the number of bits transmitted per carrier per symbol to be varied. Subcarrier modulation can be implemented using a lookup table, making it very efficient to implement.

In the receiver, mapping the received IQ vector back to the data word performs subcarrier demodulation. During transmission, noise and distortion becomes added to the signal due to thermal noise, signal power reduction and imperfect channel equalization. Figure below shows an example of a received 16-QAM signal with a SNR of 18 dB. Each of the IQ points is blurred in location due to the channel noise. For each received IQ vector the receiver has to estimate the most likely original transmission vector. This is achieved by finding the transmission vector that is closest to the received vector. Errors occur when the noise exceeds half the spacing between the transmission IQ points, making it cross over a decision boundary.

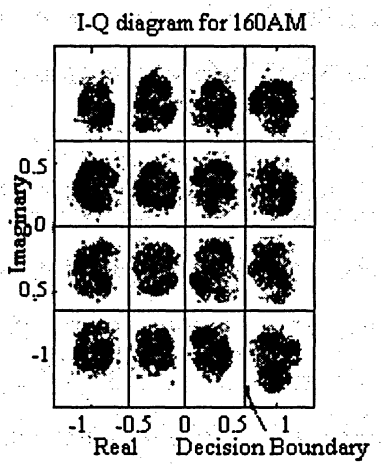

Figure 2-3, IQ plot for 16-QAM data with added noise.

2.2.3 Frequency to Time Domain Conversion

After the subcarrier modulation stage each of the data subcarriers is set to an amplitude and phase based on the data being sent and the modulation scheme; all unused subcarriers are set to zero. This sets up the OFDM signal in the frequency domain. An IFFT is then used to convert this signal to the time domain, allowing it to be transmitted. Figure below shows the IFFT section of the OFDM transmitter. In the frequency domain, before applying the IFFT, each of the discrete samples of the IFFT corresponds to an individual subcarrier. Most of the subcarriers are modulated with data. The outer subcarriers are unmodulated and set to zero amplitude. These zero subcarriers provide a frequency guard band before the nyquist frequency and effectively act as an interpolation of the signal and allows for a realistic roll off in the analog anti-aliasing reconstruction filters.

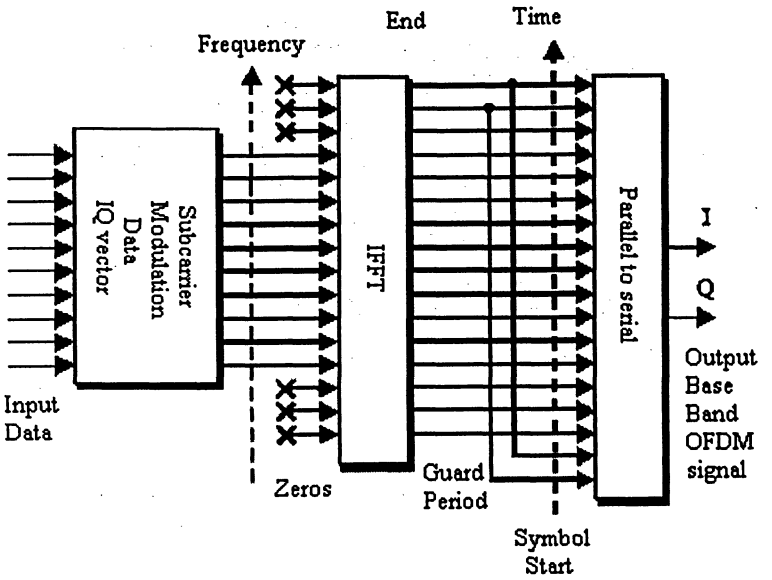

Figure 2-4, OFDM generation, IFFT stage

2.2.4 RF Modulation

The output of the OFDM modulator generates a base band signal, which must be mixed up to the required transmission frequency. This can be implemented using analog techniques as shown in Figure 2-5 or using a Digital Up Converter as shown in Figure 2-6. Both techniques perform the same operation, however the performance of the digital modulation will tend to be more accurate due to improved matching between the processing of the I and Q channels, and the phase accuracy of the digital IQ modulator.

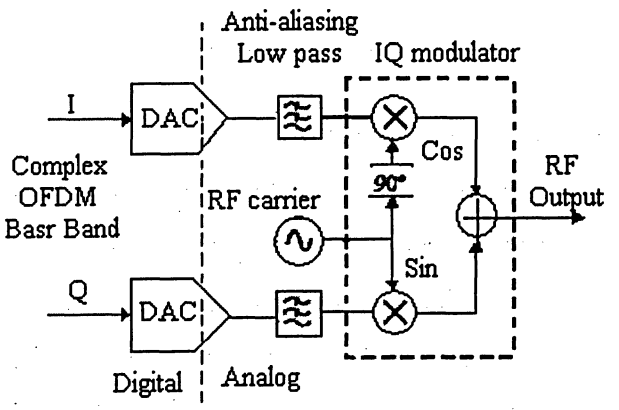

Figure 2-5, RF modulation of complex base band OFDM signal, using analog techniques.

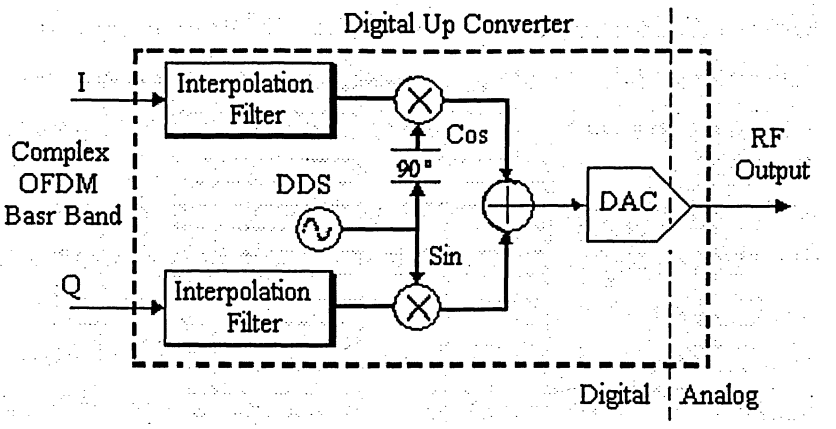

Figure 2-6, RF modulation of complex base band OFDM signal, using digital techniques.

2.3 Guard Period

For a given system bandwidth the symbol rate for an OFDM signal is much lower than a single carrier transmission scheme. For example for a single carrier BPSK modulation, the symbol rate corresponds to the bit rate of the transmission. However for OFDM the system bandwidth is broken up into N_c subcarriers, resulting in a symbol rate that is N_c times lower than the single carrier transmission. This low symbol rate makes OFDM naturally resistant to effects of Inter-Symbol Interference (ISI) caused by multipath propagation.

Multipath propagation is caused by the radio transmission signal reflecting off objects in the propagation environment, such as walls, buildings, mountains, etc. These multiple signals arrive at the receiver at different times due to the transmission distances being different. This spreads the symbol boundaries causing energy leakage between them.

The effect of ISI on an OFDM signal can be further improved by the addition of a guard period to the start of each symbol. This guard period is a cyclic copy that extends the length of the symbol waveform. Each subcarrier, in the data section of the symbol, (i.e. the OFDM symbol with no guard period added, which is equal to the length of the IFFT size used to generate the signal) has an integer number of cycles. Because of this, placing copies of the symbol end-to-end, results in a continuous signal, with no discontinuities at the joins. Thus by copying the end of a symbol and appending this to the start results in a longer symbol time. Figure 2-7 shows the insertion of a guard period.

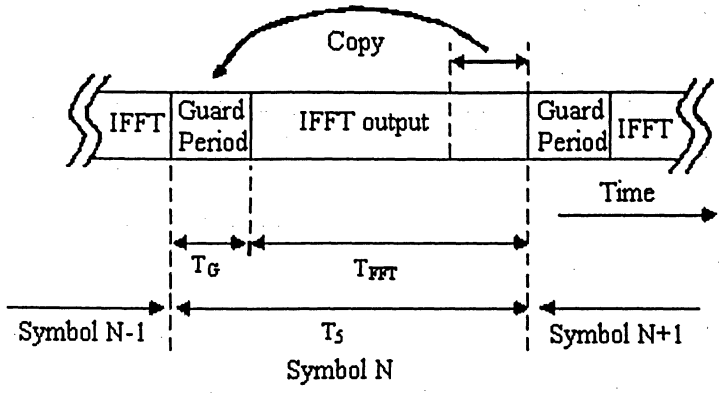

Figure 2-7, Addition of a guard period to an OFDM signal

The total length of the symbol is $T_S=T_G + T_{FFT}$, where Ts is the total length of the symbol in samples, T_G is the length of the guard period in samples, and T_{FFT} is the size of the IFFT used to generate the OFDM signal. In addition to protecting the OFDM from ISI, the guard period also provides protection against time-offset errors in the receiver.

2.3.1 Protection against Time Offset

To decode the OFDM signal the receiver has to take the FFT of each received symbol, to work out the phase and amplitude of the subcarriers. For an OFDM system that has the same sample rate for both the transmitter and receiver, it must use the same FFT size at both the receiver and transmitted signal in order to maintain subcarrier orthogonality. Each received symbol has $T_G + T_{FFT}$ samples due to the added guard period. The receiver only needs T_{FFT} samples of the received symbol to decode the signal. The remaining T_G samples are redundant and are not needed. For an ideal channel with no delay spread .The receiver can pick any time offset, up to the length of the guard period, and still get the correct number of samples, without crossing a symbol boundary. Because of the cyclic nature of the guard period changing the time offset simply results in a phase rotation of all the subcarriers in the signal. The amount of this phase rotation is proportional to the subcarrier frequency, with a subcarrier at the nyquist frequency changing by 180□for each sample time offset. Provided the time offset is held constant from symbol to symbol, the phase rotation due to a time offset can be removed out as part of the channel equalization. In multipath environments ISI reduces the effective length of the guard period leading to a corresponding reduction in the allowable time offset error.

2.3.2 Protection against ISI

In an OFDM signal the amplitude and phase of the subcarrier must remain constant over the period of the symbol in order for the subcarriers to maintain orthogonality. If they are not constant it means that the spectral shape of the subcarriers will not have the correct *sinc* shape, and thus the nulls will not be at the correct frequencies, resulting in Inter-Carrier Interference. At the symbol boundary the amplitude and phase change suddenly to the new value required for the next data symbol. In multipath environments ISI causes spreading of the energy between the symbols, resulting in transient changes in the amplitude and phase of the subcarrier at the start of the symbol. The length of these transient effects corresponds to the delay spread of the radio channel. The transient signal is a result of each multipath component arriving at slightly different times, changing the received subcarrier vector. Figure 2-8 shows this effect. Adding a guard period allows time for the transient part of the signal to decay, so that the FFT is taken from a steady state portion of the symbol. This eliminates the effect of ISI provided that the guard period is longer than the delay spread of the radio channel. The remaining effects caused by the multipath, such as amplitude scaling and phase rotation are corrected for by channel equalization.

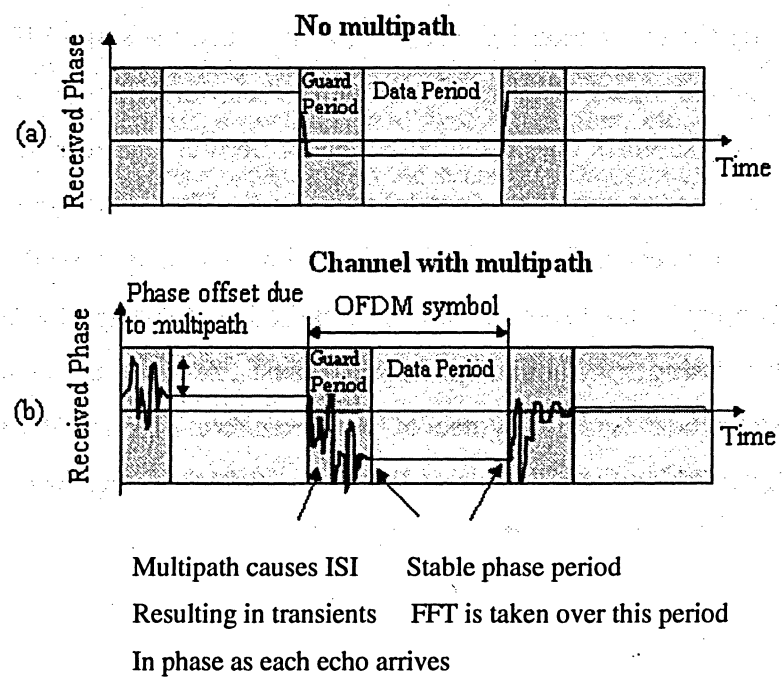

Figure 2-8, Function of the guard period for protecting against ISI.

The guard period protects against transient effects due to multipath, removing the effects of ISI, provided it is longer than the channel delay spread. This example shows the instantaneous phase of a single carrier for 3 symbols.

The addition of guard period removes most of the effects of ISI; however in practice, multipath components tend to decay slowly with time, resulting in some ISI even when a relatively long guard period is used.

In this case of an OFDM system in the presence of static multipath, the multipath impulse response followed an exponential decay with a time constant of 8 samples, resulting in an RMS delay spread of 3.5 samples. Each sample in the impulse response was complex and Gaussian distributed. The RMS delay spread is a common parameter to estimate the spread of the multipath energy in time, and used to estimate the level of ISI in single carrier communications... A more appropriate measure is the time over which 99% of the total accumulated impulse energy arrived, which in this was 16 samples.

The effective SNR of the demodulated OFDM signal is a function of the channel SNR. Effective SNR is used extensively though out this project as a measure of the performance of the communications link. It is a measure of the signal to noise ratio as seen by the OFDM receiver after demodulation, where the signal power is the magnitude of the wanted signal, and the noise is the combined error in the received signal due to all the detrimental effects in the system including channel noise, IMD, filtering, ISI, ICI, frequency errors, time offset errors, channel equalization errors, etc. The effective SNR provides a measure of the OFDM performance, independent of the modulation scheme. Traditionally the BER is used to measure the performance of a link; however in this project OFDM is considered the work with a large number of modulation schemes making BER a poor method of measurement. The BER of any particular modulation scheme can be estimated from the effective SNR by finding the BER of the modulation scheme in an AWGN channel with a SNR equal to the effective SNR In the case of multipath on the OFDM transmission, ideally the effective SNR should follow the channel SNR, however detrimental effects such as ISI lead to degraded performance. It is can see from the results that as the length of the guard period is increased the maximum effective SNR improves. For example, the effective SNR of the OFDM signal only reaches a maximum of 15 dB when the guard period length is 4 samples in length, but reaches 25 dB when a guard period of 16 samples is used. This is a result of more of the ISI

energy being removed by the guard period. This shows that having a guard period (16 samples) that is more than four times the multipath RMS delay spread (3.5 samples) still results in significant ISI. The low effective SNR for when the guard period was a similar length to the channel RMS delay spread is fine for robust modulation schemes such as BPSK and QPSK, but is insufficient for higher spectral efficiency modulation schemes such as 64-QAM and 256-QAM. Traditionally the RMS delay spread has been used as a measure of ISI and the allowable symbol rate in a multipath environment However if a higher spectral efficiency is required a more appropriate measure is needed. To achieve very high spectral efficiencies an effective SNR of greater than 35 dB must be able to be reached. In this case it required a guard period of at least 64 samples in length. This length of the guard period corresponds to the time it took for the impulse energy to decay to –35 dBc. Thus if It is require a SNR of 25 dB then there is a guard period that is at least long enough to remove all impulse reflections that are stronger than –25 dBc. When using a guard period of 64 samples, with an IFFT size of 128, and 512, in the 128-point IFFT, 80 subcarriers It is re used while in the 512-point, 320 subcarriers It is re used, making the bandwidth of both systems the same. In order for the OFDM carriers to remain orthogonal to each other, the channel response must be approximately flat over the bandwidth of each subcarrier .By using 320 subcarriers divides the channel response using finer subcarriers, and hence the variation of the channel fading over their bandwidth of each subcarrier is more constant, improving the performance. The effective SNR for the 128 IFFT size is not limited by the guard period, but instead by poor channel equalization caused by an insufficient number of subcarriers. For OFDM to operate effectively, the frequency response must be approximately flat over the bandwidth of a subcarrier. If insufficient subcarriers are used, then the frequency response changes too rapidly, leading to a degraded performance.

2.3.3 Guard Period Overhead and Subcarrier Spacing

Adding a guard period lowers the symbol rate, however it does not affect the subcarrier spacing seen by the receiver. The subcarrier spacing is determined by the sample rate and the FFT size used to analyze the received signal.

$$\Delta f = \frac{F_s}{N_{FFT}}$$

In the above Equation $\ddot{A}f$ is the subcarrier spacing in Hz, F_S is the sample rate in Hz, and $NFFT$ is the size of the FFT. The guard period adds time overhead, decreasing the overall spectral efficiency of the system.

2.4 Multiuser OFDM

DAB and DVB systems are only uni-directional from the base station to the users. Not much work has been done on using OFDM for two-way communications or for multiuser applications. These applications include wireless modems, Wireless Local Area Networks (WLAN's), Wireless Local Loop (WLL), mobile phones, and mobile high speed internet. This project aims to look at applying OFDM to such applications, and to look at the resulting advantages and problems. This project also presents some new techniques that can be used to improve broadcast and multiuser OFDM systems. This project presents the performance of adaptive modulation and adaptive user allocation schemes in a multiuser OFDM system. These techniques improve the spectral efficiency and QOS. Fattouche patented a method for implementing a wireless multiuser OFDM system in 1992, predating any published research in this field. This system used half duplex Time Division Multiplexing (TDM) to allow multiuser access, with the base stations and portable units taking turns to transmit. Carrier modulation was fixed and used D8-PSK (Differential 8 Phase Shift Keying). The system was bandwidth limited by using a raised cosine guard period. Fattouche is the founder WiLan Inc., which is one of the few companies currently producing multiuser OFDM modems. Williams and Prodan patented the use of multiuser OFDM in cable applications in 1995. This introduced the use of a hybrid user allocation, using Frequency Division Multiplexing (FDM) and TDM. In this system the users are allocated in time and frequency slots depending on the data demand. This patent however, fails to address problem of obtaining and maintaining accurate time and frequency synchronization between users, which is critical for maintaining orthogonality between users. Cimini, Chuang, Sollenberger [98] outlined an Advanced Cellular Internet Service using multiuser OFDM. The aim of this system was to provide Internet access at a data rate of 1 – 2 Mbps. This system uses time synchronized base stations, which are allocated time slots in a self-organizing fashion. These base station time slots are then broken down in to time slots for users. In addition to TDM, users are allocated subcarriers dynamically based on the channel Signal to Interference Ratio (SIR), to allow minimization of inter-cellular interference.

Wahlqvist [35] described one possible implementation of multiuser OFDM in a wireless environment, outlining a user allocation scheme where users are allocated small blocks of time and frequency. In this scheme, each transmission block consists of a small group of subcarriers, (5 - 10) and a small number of symbols, about 11 in length. The aim of this structure is to allocate time and frequency slots to utilize the high correlation between neighbouring subcarriers, and the small channel variation between a small group of symbols. This allows the block to be characterized with a simple pilot tone structure.

3. RADIO-OVER-FIBER (RoF)

RoF techniques are attractive schemes for realizing seamless wireless networks since they allow for the easy distribution of microwaves and millimeter waves over long distances along optical fibers [44]–[46]. One of the many benefits of RoF techniques is that almost all of the expensive wireless parts can be centralized in a center station (CS). As a result, the system can be easily maintained and small-sized remote antenna units (RAUs) can be built, allowing RAUs to be installed in confined spaces such as underground cities and tunnels. By using these advantages, RoF systems have already been introduced into several cellular systems using a 1–2-GHz band [47]–[50] including the personal digital cellular (PDC) system and the code division multiple access (CDMA) system.

In recent years, popularity of the wireless local area network (WLAN) has been growing rapidly because WLAN technology offers easy high-speed access to the Internet. As a result, wireless local area network access points (WLAN APs) have been installed in many areas, creating a number of operations and maintenance problems. For example, without the careful management of channel allocation, serious radio interferences can be caused. Even when the channel allocation is managed by an administrator, the existence of several different WLAN standards such as IEEE802.11a [51], 11b [52], 11g, 11i, and 11e result in more complicated transmission characteristics. It is proposed that the application of RoF techniques to WLAN systems [53], [54] as a solution to these problems.

To introduce RoF techniques to higher frequency wireless systems such as a WLAN, optical devices [laser diodes (LDs) and photo diodes (PDs)] with high-frequency responses of more than 5 GHz are generally required. However, in consumer applications, reducing the cost of these optical devices is essential.

3.1 ROF system

RoF is a technology by which microwave (electrical) signals are distributed by means of optical components and techniques. A RoF system consists of a Central Site (CS) and a Remote Site (RS) connected by an optical fiber link or network. One of the major motivation and system requirements for RoF technology is the use simple and cost- effective RS [45].

The electrical signal distributed may be baseband data, modulated IF, or the actual modulated RF signal. The electrical signal is used to modulate the optical source. The resulting optical signal is then carried over the optical fiber link to the remote station. By delivering the radio signals directly, the optical fiber link avoids the necessity to generate high frequency radio carriers at the antenna site. Since antenna sites are usually remote from easy access, there is a lot to gain from such an arrangement. However, the main advantage of RoF systems is the ability to concentrate most of the expensive, high frequency equipment at a centralized location, thereby making it possible to use simpler remote sites [46].

3.2 RoF and Modulation

For the future wireless access networks, microwave and millimeter-wave band radio over fiber (RoF) systems can be applied combined with dense wavelength-division multiplexing (DWDM) [44]–[50]. To improve optical spectral efficiency in transmission and reduce chromatic dispersion impact on transmission, two subcarrier modulations (SCMs), i.e., single-sideband modulation (SSB) and tandem single-sideband (TSSB) modulations, It is proposed and demonstrated [51]–[53]. The two SCMs both can be realized by using optical Mach–Zehnder modulators (MZMs), which have a cosine transfer function theoretically in the electric field domain. In other words, MZMs have the nonlinear transfer function, leading to nonlinear distortion consisting of harmonic distortion (HD) and intermodulation distortion (IMD) when radio frequency (RF) signals electrically drive an MZM. The IMDs can be further increased when multiple RF signals or frequency division-multiplexed (FDM) signals drive an MZM simultaneously (i.e., one wavelength carries multiple RF signals). Such nonlinear distortions will considerably reduce receiver sensitivity and dynamic range, and thus, RoF system performance [46], [54]–[56]. For the SSB SCM, multiple RF or FDM signal tones carried by one wavelength or optical carrier are located in either lower sideband (LSB) or upper sideband (USB) of the optical carrier, whereas for the TSSB SCM, one half of multiple RF signals or FDM signal tones are located in LSB and the others in USB of the optical carrier. Therefore, the optical spectral efficiency with both SCMs can be the same in DWDM RoF systems. Intuitively, it should be expected that the two SCMs should result in similar nonlinear distortion for a similar RoF system setup. However, it will show that nonlinear distortions in RoF systems using the SSB and TSSB SCMs may be different,

strongly depending on optical modulation index and frequency difference of two RF signals as we see as in transmission fiber.

To achieve high-capacity wireless access networks, very dense WDM systems have to be used, which can be combined with microcell and picocell wireless networks. Therefore, we mainly focus on the analysis of nonlinear distortion in DWDM RoF systems with optical channel spacing of 12.5 GHz. However, our theory and analysis can be easily modified and applied for DWDM channel spacing of 25 GHz. In addition, the impact of nonlinear distortion was investigated only for DWDM RoF systems using SSB SCM with a small modulation index [46]. However, a large modulation index is usually preferred in RoF systems, but serious nonlinear distortion may be induced. A detailed investigation of nonlinear distortion in RoF systems with TSSB and SSB SCMs has not been given so far.

4. OFDM-ROF system

4.1 System Model

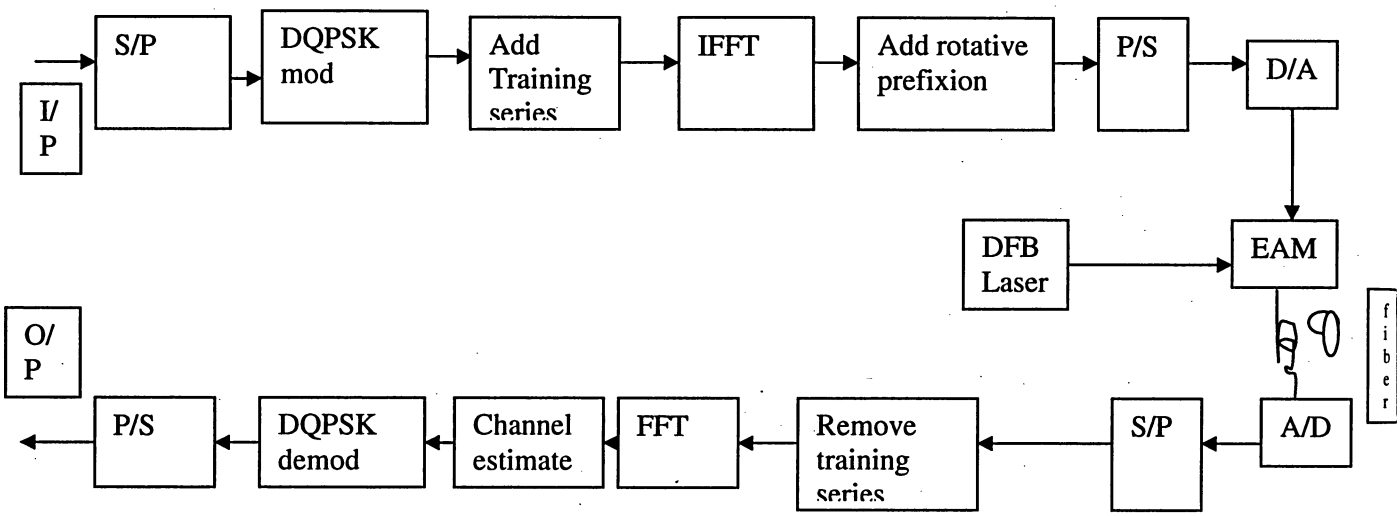

Fig 4-0: OFDM –RoF System Model

4.2 System Description

Let $A \triangleq \{A_0, A_1 \ldots, A_{N-1}\}$ denote an encoded data sequence to be transmitted for one OFDM symbol with N sub-carriers, where A_k represents the complex data of the kth sub-carrier. The complex baseband OFDM symbol (centered at zero frequency) is expressed as

$$s(t) = \frac{1}{\sqrt{N}} \sum_{k=0}^{N-1} A_k e^{j2\pi(k-(N-1)/2)t/T_s}, \quad 0 \le t < T_s \tag{1}$$

where T_s is the symbol period of the OFDM signal.

Consider the above OFDM symbol sampled at the sampling period. $\triangle t = T_s / JN$. The discrete-time OFDM signal sampled at time instant $t = n\triangle t$ is then expressed as

$$s_n \triangleq s(n\Delta t) = e^{j\varphi_{J,n}} \frac{1}{\sqrt{N}} \sum_{k=0}^{N-1} A_k e^{j2\pi k(n/JN)} \tag{2}$$

where $n = 0\ 1, JN - 1$, and $\varphi_{J,n}$ is the frequency offset [24] given by

$$\varphi_{J,n} \triangleq \frac{n(1-N)}{JN}\pi \tag{3}$$

The frequency offset introduced here is mainly for analytical purpose; the offset guarantees the power spectrum of the input base-band signal to be conjugate symmetric, which will simplify the derivation of the SDR of the clipped base band OFDM signal discussed later in Section IV and the Appendix. When N is odd, of course, a proper assignment of the subcarriers renders the offset unnecessary. In any case, the offset is immaterial to our analysis of peak power, since it does not change the amplitude of the complex envelope.

The parameter can be considered as an oversampling factor and the clipping system with $J = 1$ is called the Nyquist-rate clipping, which is the case exclusively discussed in [60].

Although we assume J an integer in the following for simplicity, the parameter J need not be an integer, as long as JN is. Also in practice, JN should be chosen as a power of two such that the fast Fourier transform (FFT) algorithm can be employed for computational reduction.

Note that the above equation can be also expressed as

$$s_n = e^{j\varphi_{J,n}} \cdot \frac{\sqrt{J}}{\sqrt{JN}} \sum_{k=0}^{JN-1} A_k^1 e^{j2\pi k(n/JN)} \tag{4}$$

where

$$A_k^1 = \begin{cases} A_k, & \text{for } k < N, \\ 0, & \text{for } k \geq N. \end{cases} \tag{5}$$

Equations (4) and (5) indicate that the continuous OFDM (without frequency offset) can be approximated by using the JN point inverse discrete Fourier transform (IDFT) of the zero padded sequence of length JN, i.e.,

$$s_n = e^{j\varphi J,n}\, s_n^J \tag{6}$$

where

$$s_n^J \triangleq \sqrt{J}\, IDFT\,(JN, A^J)_n \tag{7}$$

and

$$A^1 \triangleq \{A_0, A_1, \ldots, A_{N-1}, \underbrace{0,0,\ldots,0}_{(J-1)\,N\,0's}\}. \tag{8}$$

Throughout the project, the DFT and IDFT operations are defined as follows; the nth output of the L-point DFT and IDFT of the complex-valued input $X = [X_0, X1, X_{L-1}]$ are given, respectively, by

$$DFT(L,X)_n \triangleq \frac{1}{\sqrt{L}} \sum_{k=0}^{L-1} X_k e^{-j2\pi(k/L)n},$$

$$IDFT(L,X)_n \triangleq \frac{1}{\sqrt{L}} \sum_{k=0}^{L-1} X_k e^{j2\pi(k/L)n}.$$

Also, the data A_k are assumed to be zero-mean random variables with reasonable statistical independence such that the OFDM signal approaches a complex zero-mean Gaussian process for large N.

4.2.1 Soft Envelope Limiter

Let $r_n e^{j\varphi n}$ denote the input complex signal s_n in polar coordinates. As a clipping model of the base-band signal, it is consider the following soft envelope limiter; the nth output sample is given by $\tilde{s}_n = \tilde{r}_n e^{j\varphi n}$ with

$$\tilde{r}_n = g(r_n) \triangleq \begin{cases} r_n, & \text{for } r_n \le A_{max} \\ A_{max}, & \text{for } r_n > A_{max} \end{cases} \tag{9}$$

where A_{max} is the maximum permissible amplitude over which the signal is clipped. The clipping ratio γ is defined as

$$\gamma \triangleq \frac{A_{max}}{\sqrt{P_{in}}} \tag{10}$$

Strictly speaking, the use of channel coding may result in the statistical dependence of the encoded data A_k.

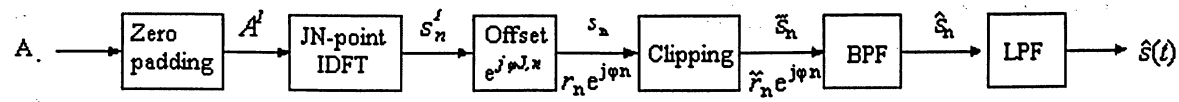

(a)

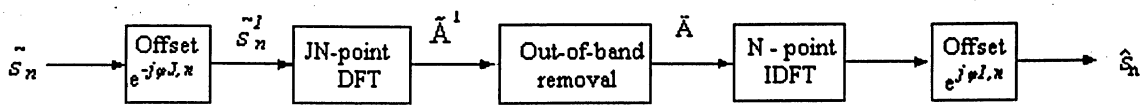

(b)

Fig. 4-1. OFDM system with soft envelope limiter. (a) Transmitter. (b) The low-pass equivalent BPF.

where P_{in} is the average input power of the OFDM signal before clipping.

Obviously, the clipping process reduces the output power and let P_{out} denote the average output power *after the soft envelope limiter*. Now, assuming that the OFDM signal is complex Gaussian, which may be valid in the case of OFDM signals with large N, the amplitude γ_n is Rayleigh distributed and it can be easily shown that the average output power is given by [60], [82].

$$P_{out} = (1 - e^{-\gamma^2})\, P_{in} \tag{11}$$

Following [60], for convenience of notation, It is define $\gamma = 0$ as a hard (constant) envelope limiter and $\gamma = \infty$ as an ideal system without clipping. In fact, the amplitude of the signal normalized by the rms average output power after the hard envelope limiter is upper bounded as

$$\begin{aligned} \lim_{\gamma \to 0} \frac{|\tilde{s}_n|}{\sqrt{P_{out}}} \le \lim_{\gamma \to 0} \frac{A_{max}}{\sqrt{P_{out}}} &= \lim_{\gamma \to 0} \frac{\gamma \sqrt{P_{in}}}{\sqrt{(1 - e^{-\gamma^2})\, P_{in}}} \\ &= \lim_{\gamma \to 0} \frac{\gamma}{\sqrt{1 - e^{-\gamma^2}}} = 1 \end{aligned} \tag{12}$$

but, since, $\sum_{n=0}^{JN-1} |\tilde{s}_n|^2 / JN = P_{out}$ .It follows that

$$\lim_{\gamma \to 0} \frac{|\tilde{s}_n|}{\sqrt{P_{out}}} = 1 \quad \text{for } n = 0,1,\ldots, JN-1 \tag{13}$$

which justifies the output signal to have a constant envelope.

4.2.2 Low-Pass Equivalent Bandpass Filter

As a band-pass filter (BPF) for the removal of the out-of-band radiation caused by the clipping, It is consider the following low-pass equivalent rectangular BPF. After the soft envelope limiter and frequency shift, the signal is processed by the *JN*-point DFT which yields the distorted data sequence of length *JN*

$$\tilde{A}^{I} \triangleq \{ \tilde{A}_0, \tilde{A}_1, \ldots, \tilde{A}_{N-1}, \underbrace{\tilde{A}_N, \ldots, \tilde{A}_{JN-1}}_{\text{out-of-band}}$$

where

$$\tilde{A}_k = \mathrm{DFT}(JN, \{\tilde{s}_n^{-1}\})_k \tag{14}$$

is the distorted version of the original data A_k and. $\tilde{S}_n^{I} \triangleq e^{-j\varphi_{J,n}} \tilde{s}_n$. Pruning the out-of-band components, one may obtain the distorted version of the original data sequence of length $N\tilde{A} = \{ \tilde{A}_0, \tilde{A}_1, \ldots, \tilde{A}_{N-1} \}$.

This sequence is modulated as usual by the N - point IDFT, expressed as (6) with $J \equiv 1$, i.e.

$$\hat{s}_n = e^{j\varphi 1,n}\, IDFT(N,\tilde{A})_n. \tag{15}$$

The low-pass equivalent BPF process described above is outlined in Fig. 1(b). Implementing the clipping system as above may completely eliminate the out-of-band radiation caused by the clipping regardless of the oversampling factor *J*. Thus, the spectral requirement of this system becomes the same as that of an unclipped OFDM system, provided that the HPA is operated with a linear region. Also, the entire BPF process becomes meaningless and thus can be omitted for the Nyquist-rate clipping system (J = 1), in which case one simply has $\hat{s}_n = \tilde{s}_n$. The output power of the clipped OFDM signals *after the BPF* is given by

$$\hat{P}_{av} \triangleq \frac{1}{N} \sum_{k=0}^{N-1} E\left[|\tilde{A}_k|^2 \right] \tag{16}$$

where E[.] denotes the expectation operation.

The average output power after the BPF is generally lower than the output power before the BPF, i.e., $\hat{P}_{av} \leq P_{out}$ and the equality holds if and only if $J = 1$ or $\gamma = \infty$. Thus, it is define a reduction ratio of the total power by the BPF as

$$\beta \triangleq \frac{\hat{P}_{av}}{P_{out}} = \frac{\sum_{k=0}^{N-1} E\left[|\ddot{A}_k|^2\right]}{\sum_{k=0}^{JN-1} E\left[|\ddot{A}_k|^2\right]} \leq 1 \tag{17}$$

After the ideal LPF and D/A conversion, the band-limited signal is expressed as

$$\hat{s}(t) = LPF\,[\hat{s}_n] \tag{18}$$

where $LPF[.]$ denotes the ideal low-pass filtering (including D/A conversion) of the discrete samples. Finally, the complex baseband signal is upconverted and amplified by the HPA.

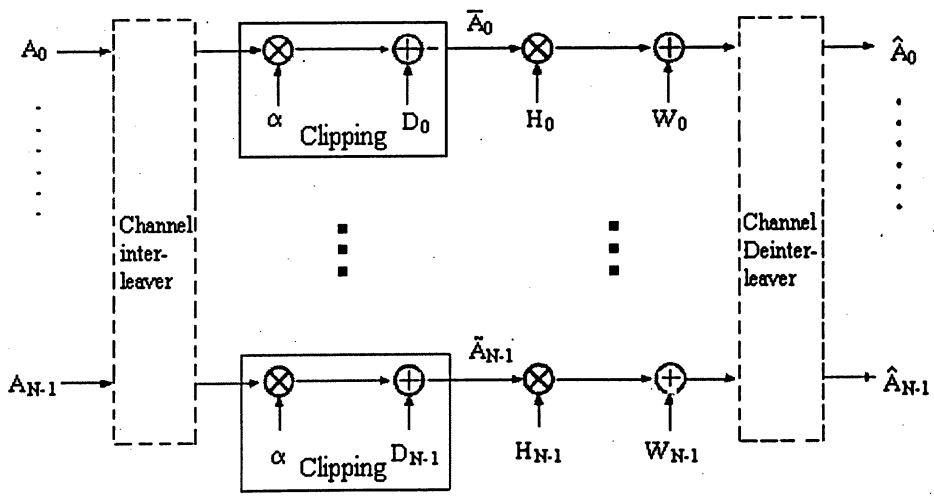

Fig 4-2. Channel model.

4.2.3 Channel and Receiver Model

It is consider the conventional DFT-based receiver for detection of the OFDM signal. At the receiver, the received analog signal is low-pass filtered and sampled at the Nyquist rate and the samples are processed by the N-point DFT to retrieve the original data. In the following, the perfect synchronization and the perfect carrier recovery is assumed. It is also assumed that the clipped signal after filtering is linearly amplified.

The sampled signal at the receiver is expressed as

$$z_n = h_n \otimes \hat{s}_n + \omega_n, \qquad \text{for } n = 0,1,\ldots, N-1 \tag{19}$$

where h_n and w_n are complex channel impulse response and zero-mean complex Gaussian noise, respectively, and $\otimes$ denotes the convolution.

For an AWGN channel, the received data of the kth subcarrier is given by

$$\hat{A}_k = DFT\,(N, \{e^{-j\varphi l,n} Z_n\})_k = \tilde{A}_k + W_k \tag{20}$$

where W_k is the AWGN term that falls on the kth subcarrier.

For a fading channel, the received data can be modeled as

$$\hat{A}_k = H_k \tilde{A}_k + W_k \tag{21}$$

where H_k is a channel coefficient of the kth subcarrier. With a sufficient guard interval of OFDM signals, the effect of the intersymbol interference (ISI) caused by the dispersive fading channel can be neglected. In this project, It is assume that the symbol-wise (i.e., subcarrier-wise) channel inter leaver (both in frequency and time domain) is ideal such that the channel is characterized as memoryless and the fading is slow and Rayleigh [83].It is also assume that H_k is known to the receiver *a priori*, i.e., the perfect channel state information (CSI) is available. Consequently, at the channel decoder the H_k are modeled as real-valued and statistically independent Rayleigh random variables [84] and the index k is dropped from H_k in the following. The received data to be processed by the channel decoder can now be expressed as

$$\hat{A}_k = H\tilde{A}_k + W_k \tag{22}$$

where H is an independent and identically distributed (i.i.d.) Rayleigh random variable which is known at the receiver (perfect CSI). The channel model considered throughout the project for the evaluation of performance degradation is shown in Fig.4- 2. The parameters in the figure such as $\propto$ and D_k are defined in Section IV.

5. PEAK TO AVERAGE POWER RATIO AND INSTANTANEOUS POWER

For wireless applications, efficient power amplification is required to provide adequate area coverage and to minimize battery consumption. The conventional solutions to the PAPR problem are to use a linear amplifier or to back-off the operating point of a nonlinear amplifier; both approaches resulting in a significant power efficiency penalty. Several alternative solutions have been proposed to reduce the PAPR. The simplest of these approaches is to deliberately clip the OFDM signal before amplification [67-68], which gives a good PAPR but at the expense of some performance degradation. Another uses nonlinear block coding [99], where the desired data sequence is embedded in a larger sequence and only a subset of all the possible sequences are used, specifically, those with low peak powers. Using this approach, a 3-dB PAPR can be achieved with only a small bandwidth penalty. As originally described, to implement this coding scheme, large look-up tables are required at the transmitter and the receiver, limiting its usefulness to applications with a small number of subchannels, progress has been made towards coding schemes that reduce the PAPR, can be implemented in a systematic form, and have some error correcting capabilities [100]. Nevertheless, these methods are difficult to extend to systems with more than a few subchannels and the coding gains are small for reasonable levels of redundancy. Another, two promising techniques for improving the statistics of the PAPR of an OFDM signal are the Selective Mapping approach(SLM) and the Partial Transmit Sequence(PTS) approach [91],[101] . Both introduce additional complexity but provide improved PAPR statistics for the OFDM signal with little cost in efficiency.

5.1 Peak-to-Average Power Ratio (PAPR)

The PAPR of the complex base-band OFDM signals is defined as

$$P \triangleq \max_{0\le t<T_s} \frac{|\hat{s}(t)|^2}{\hat{P}_{av}} = \max_{0\le t<T_s} \frac{|LPF[\hat{s}_n]|^2}{\hat{P}_{av}} \qquad (23)$$

The above expression requires the knowledge of $\hat{P}_{av}$, i.e., the average power after the BPF, defined in (16), which has to be calculated

An alternative definition is

$$P \triangleq \max_{0 \le t < T_s} \frac{|LPF[\hat{s}_n]|^2}{\hat{P}} \tag{24}$$

where $\hat{P}$ is the average power of a given sample OFDM symbol defined as

$$\hat{P} \triangleq \frac{1}{N} \sum_{k=0}^{N-1} |\tilde{A}_k|^2 \tag{25}$$

Note the difference of the average power between (16) and (25).While the average power of (16) is constant; the above value in (25) is a random variable due to the fact that the A_k are random variables. However, these two definitions of the PAPR may converge for large [85].

5.2 Instantaneous Power

In addition to the PAPR of the clipped OFDM signal, It is also evaluate the instantaneous power of the clipped and band-limited OFDM signal normalized by the average power, i.e. $\zeta(t) \triangleq |\hat{s}(t)|^2 / \hat{P}_{av}$ Without clipping, since $s(t)$ is a complex Gaussian random process by assumption, $\zeta(t)$ is chi-square distributed with one degree of freedom. Consequently, the complementary cumulative distribution function (cdf) of $\zeta(t)$ is given by the exponential function, i.e., $\Pr[\zeta(t) > \zeta_0] = e^{-\zeta_0}$ for any given time instant t. On the other hand, the statistical distribution of the instantaneous power of the clipped and band-limited OFDM signal considered in this project depends on the time instant t, where $0 \le t < T$, $T \triangleq T_s/N$, being the Nyquist interval of the signal, due to the fact that the clipped and band-limited OFDM signal becomes cyclo-stationary with period T [85].

5.3 Methods of reducing PAPR

5.3.1Deliberate Clipping

In this method [96] the number of subcarriers is 512 and each sub carrier is modulated by quadrature phase shift keying (QPSK).

The resultant complementary cdf [96] is shown in Fig 5-1 in the case of γ= 0 and 1.0. Also shown in the figure is the analytical approximation of the complementary cdf of the PAPR without clipping obtained from [86]. It is observed that even though the Nyquist-rate clipping considerably reduces the PAPR compared to that without clipping, the clipping with oversampling yields significantly lower PAPR than that without oversampling. In particular, the difference between the PAPR of J=16 and that of J = 1 is as large as about 2–3 dB, which is quite noticeable. Thus, the results of [96] suggest that the over-sampling of the OFDM signal prior to the clipping may be effective in reducing the PAPR of the band-limited OFDM signals.

With the same setup, the complementary cdf of the instantaneous power of the hard-envelope-limited OFDM signal normalized by the average power is obtained with various over-sampling factor J. It is choose the time instant $t = T/2$, since the most significant fluctuation of the complex envelope caused by the LPF may be observed in the middle of the clipped discrete samples. The result is shown in Fig 5-2. As a reference, the instantaneous power of the OFDM signal without clipping is also plotted. Analogous to the case of the PAPR, a noticeable regrowth of the instantaneous power is observed in the case of the Nyquist-rate clipping.

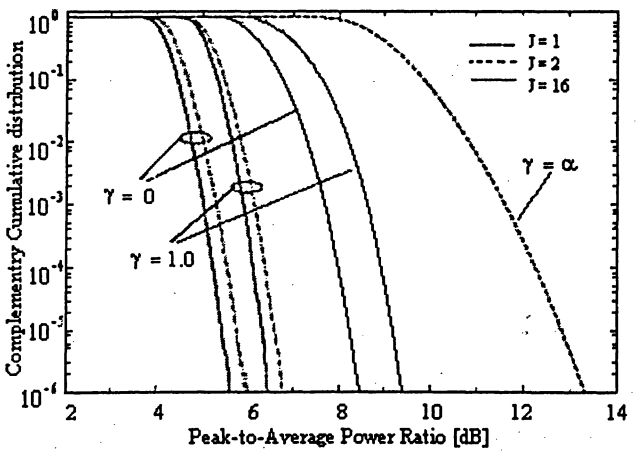

Fig. 5-1 Comparison of the complementary cdf of the PAPR of the clipped and band-limited OFDM signals with oversampling factor J = 1, 2, and 16 (N =512, QPSK). [96]

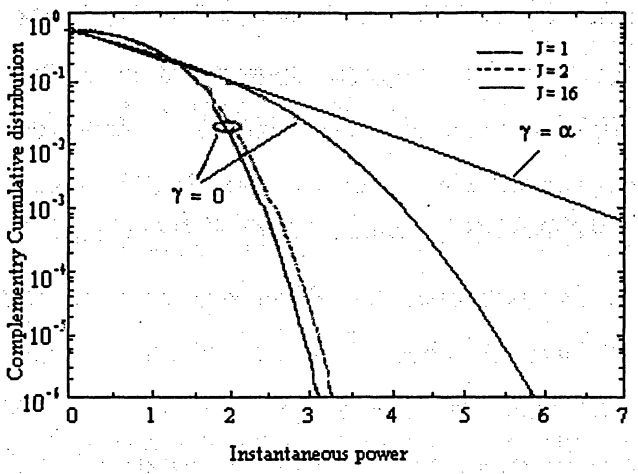

Fig. 5-2 Comparison of the complementary cdf of the instantaneous power of hard-envelope-limited and band-limited OFDM signals with J = 1, 2, and 16(N = 512, QPSK) at the time instant t = T=2. [96]

The Nyquist-rate clipping results in such high peak power re-growth because of the clipped samples $\hat{s}_n$ become statistically independent, while the samples of the clipped signal with oversampling generally have statistical dependence such that the clipped continuous signal is reconstructed. Also, with the help of Gaussian approximation, the mathematical description of the Nyquist-rate clipping is available due to the statistical independence of the samples and thus the distribution of the instantaneous power is also analytically tractable, even though it may not be given in a simple closed-form expression. In [85], [87], a tight lower bound of the complementary cdf of the instantaneous power is derived, which can be numerically calculated. The distribution of the instantaneous power for this case is referred to [84], [87].

5.3.2 Selective Mapping

In the *SLM* approach [90], *M* statistically independent sequences are generated from the same information and that sequence with the lowest *PAPR* is chosen for transmission. In the ***SLM*** implementation shown in fig below, $\boldsymbol{M}$ transmit sequences are produced by multiplying the information sequence by $\boldsymbol{M}$ random sequences of length ***N***. If the *CCDF* of the original sequence is *Pr (PAP >PAP,),* then, the *CCDF* of the best of the $\boldsymbol{M}$ sequences will be *[Pr (PAP>PAP,) IM.* Thus, in theory, the probability of the *PAP* exceeding some threshold can be made as small as possible at the expense of added complexity (i.e., additional IFFTs).

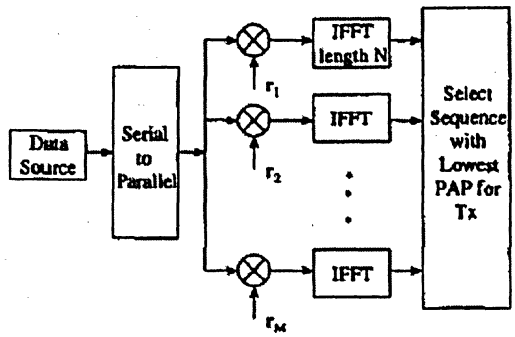

Fig 5-3 SLM approach

To recover the data, the receiver must know which "multiplying" sequence has been used; this can be transmitted as side information

5.3.3 Partial Transmit Sequences

In the *PTS* approach [91], the input data block is partitioned into disjoint subblocks or clusters which are combined to minimize the *PAP*. Define the data block, *{X, n=O, l,* ..., N-1), as a vector, **X=[Xo** XI ... *X N - , I T*. Then, partition **X** into *M* disjoint sets, represented by the vectors {X, m = 1,2 ,... *, M) ,* such that

$$\mathbf{X} = \sum_{m=1}^{M} \mathbf{X}_m$$

Here, it is assumed that the clusters consist of a contiguous set of subcarriers and are of equal size. The objective of the *PTS* approach is to form a weighted combination of the *M* clusters,

$$\mathbf{X}' = \sum_{m=1}^{M} b_m \mathbf{X}_m$$

where {bm,m=1,2, ..., *M]* are weighting factors i,m,d are assumed to be pure rotations. After transforming to the time domain, the above equation becomes

$$\mathbf{x}' = \sum_{m=1}^{M} b_m \mathbf{x}_m$$

The vector x, called the *partial transmit seguenets,* is the IFFT of X, The phase factors are then chosen to minimize the *PAP* of **x'.** As for the *SLM* technique, in the *PTS* approach, the receiver must have knowledge about the generation process of the transmitted OFDM signal.

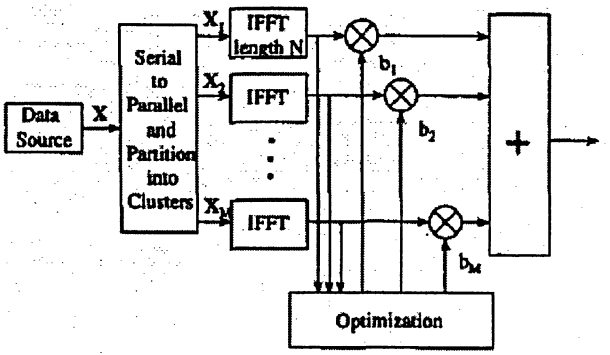

Fig 5-4 PTS approach

The phase factors must then be transmitted as side information resulting in some loss of efficiency. Alternatively, differential encoding can be employed across the subcarriers within a cluster; in this case, the overhead is a single reference subcarrier per cluster It is shown in [91] that, using 128 subcarriers with four clusters and phase factors limited to the set **{+1** *,kj},* the 1% ***PAP*** can be reduced by more than **3** dB.

An important advantage of this technique, and of the SLM approach, is that it applies to an arbitrary number of subcarriers and to any size signal constellation. In [90], using 128 subcarriers and ***M=4,*** with values chosen from the set, it is shown that the 1% *PAP* (i.e., the *PAP* exceeds this value for less than 1% of the OFDM blocks) can be reduced **by** more than 2 dB. It **is** advantageous to choose sequences with values limited to the set (&l, &j}, since phase shifts by multiples of n/2 can be implemented without any multiplications.

6. SIGNAL DISTORTION RATIO AND CHANNEL CAPACITY

The effect of the clipping on OFDM signal in terms of degradation in SDR and channel capacity are based on the assumption that the OFDM signal samples s_n are characterized as a discrete complex stationary Gaussian process.

6.1 Signal-to-Distortion Ratio (SDR)

Suppose that the Gaussian process s_n is input to the channel with memoryless nonlinearity. Applying the special case of Price's theorem for Gaussian inputs [73], known as Bussgang's theorem, one can write the output as [82]

$$\tilde{s_n} = \alpha s_n + d_n \quad \text{for } n = 0,1,\ldots, JN-1 \tag{26}$$

where the distortion term d_n is uncorrelated with S_n and the attenuation factor $\propto$ is calculated for the soft envelope limiter as [60], [82]

$$\alpha = \frac{E[s_n^* \tilde{s_n}]}{E[|s_n|^2]} = \frac{E[r_n g(r_n)]}{E[|r_n|^2]} = 1 - e^{-\gamma^2} + \frac{\sqrt{\pi}\gamma}{2}\text{erfc}(\gamma). \tag{27}$$

Consequently, the data at the kth subcarrier after the JN -point DFT is written as

$$\begin{aligned}
\tilde{A}_k &= DFT(JN, \{\tilde{s}_n\})_k \\
&= \frac{1}{\sqrt{JN}} \sum_{n=0}^{JN-1} e^{-j\varphi J,n} \tilde{s}_n e^{-j2\pi(k/JN)n} \\
&= \underbrace{\alpha \frac{1}{\sqrt{JN}} \sum_{n=0}^{JN-1} e^{-j\varphi J,n} s_n e^{-j2\pi(k/JN)n}}_{A_k} \\
&\quad + \underbrace{\frac{1}{\sqrt{JN}} \sum_{n=0}^{JN-1} e^{-j\varphi J,n} d_n e^{-j2\pi(k/JN)n}}_{D_k}
\end{aligned} \tag{28}$$

where D_k is the complex distortion term falls on the kth subcarrier. The D_k can be seen as a sum of random variables that are not necessarily statistically independent. However, as a consequence of the central limit theorem that may hold for large classes of even dependent variables [89], It is empirically assume D_k as Gaussian in the sequel, which is the common assumption when N is large [71], [75]–[79]. The Gaussian distribution corresponds to, in effect, the worst kind of additive noise in view of channel capacity and thus assuming the distortion terms Gaussian independent of the input signal may serve as a lower bound in terms of the channel capacity. Note, however, that results show that with good accuracy the distortion terms approach Gaussian for relatively large N.

Strictly speaking, even under the assumption that the D_k are Gaussian, the D_k are statistically dependent in general. In this project, however, It is treat each sub-carrier as an independent channel and on this basis all the modulation-detection processes are carried out as is often the case with the practical OFDM systems. That is, we do not consider the joint detection of the distortion terms D_k at the receiver for possible performance improvement. The channel interleaving and de-interleaving may also eliminate the statistical dependence of the distortion terms. Thus, the channel capacity will be calculated assuming the statistical independence between sub-carriers.

Now the SDR of the k^{th} sub-carrier is given by

$$\mathrm{SDR}_k = \frac{E[|\alpha A_k|^2]}{E[|D_k|^2]} = \alpha^2 \frac{P_{in,k}}{P_{d,k}} \tag{29}$$

where $P_{in,k} \triangleq E[|A_k|^2]$ is the average power of the k^{th} subcarrier before clipping and $P_{d,k} \triangleq E[|D_k|^2]$ is the average power of D_k which can be obtained by deriving the power spectral density(PSD) of the distortion component. In order to incorporate the hard envelope limiter as a special case, we rewrite SDR_k as

$$\mathrm{SDR}_k = \frac{\alpha^2 \dfrac{P_{in,k}}{P_{d,k}}}{\dfrac{P_{out}}{P_{out}}} = K\gamma \frac{\dfrac{P_{in,k}}{P_{in}}}{\dfrac{P_{d,k}}{P_{out}}} \tag{30}$$

where a normalized attenuation factor K_γ is defined as [60]

$$K\gamma \triangleq \frac{\alpha^2 P_{in}}{P_{out}} = \frac{\alpha^2}{1-e^{-\gamma^2}} \tag{31}$$

Note that for the hard envelope limiter, $K\gamma$ is given by its limit $\lim_{\gamma \to 0} K\gamma = \pi/4$, while for an ideal channel $\lim_{\gamma \to \infty} K\gamma = \pi/1$..

6.2 Channel Signal-to-Noise Ratio

We define the channel SNR as a ratio of the average power of the modulated signal (i.e., useful signal plus distortion) to the average power of Gaussian noise over the effective bandwidth both measured at the receiver input, i.e.,

$$\mathrm{SNR}_c \triangleq \frac{\hat{P}_{av}}{P_{noise}} = \beta \frac{P_{out}}{P_{noise}} \tag{32}$$

where $\hat{P}_{av}$ and P_{noise} are the average power of the output signal [defined in (16)] and the AWGN at the receiver (i.e., *after* the rectangular filter), respectively. The reduction ratio β, defined in (17), is expressed using (29)–(31) as

$$\beta = K\gamma \left\{ 1 + \sum_{k=0}^{N-1} \frac{P_{in,k}}{P_{in}\,\mathrm{SDR}_k} \right\} \tag{33}$$

If all the sub-carriers have equal power, i.e., $P_{in,k} = P_{in}/N$ for all k, then (33) reduces to

$$\beta = K\gamma \left\{ 1 + \frac{1}{N} \sum_{k=0}^{N-1} \mathrm{SDR}_k^{-1} \right\} \tag{34}$$

which is a function of the sum of SDR_k^{-1}.

6.2.1 *Channel Capacity over an AWGN Channel*

Now It is derive the channel capacity[5] of the clipped OFDM signals under the assumption that the distortion terms are uncorrelated additive Gaussian random variables. Our definition of the channel capacity is in bits *per sub-carrier*, focusing on degradation in the required SNR_c compared to an ideal system without clipping.

Recall that from (20) and (28) the received kth signal after the DFT is given by the sum of the attenuated signal plus the additive noise

$$\hat{A}_k = \alpha A_k + Z_k \tag{35}$$

where $Z_k = D_k + W_k$. Since the distortion component D_k is assumed complex Gaussian with zero mean, the additive noise Z_k can be characterized as a zero-mean complex Gaussian random variable with variance $E[|Z_k|^2] = E[|D_k|^2] + E[|W_k|^2]$, statistically independent of the input signal.

Given the input power of the kth sub-carrier $P_{in,k}$ and without any constraint on the distribution of the signal constellation, the channel capacity of the kth subcarrier over an AWGN channel is expressed as

$$C_k = \max_{P_{in,k}} I(A_k; \hat{A}_k) = h(\hat{A}_k) - h(Z_k) = \log_2(1 + \mathrm{SNDR}_k) \tag{36}$$

where $I(X;Y)$ is the mutual information between X and Y and $h(X)$ denotes the differential entropy of the complex-valued signal . The signal-to-noise-plus-distortion ratio (SNDR)of the k^{th} subcarrier is given by

$$\begin{aligned} \mathrm{SNDR}_k &= \frac{E[|\alpha A_k|^2]}{E[|D_k + W_k|^2]} \\ &= \frac{\alpha^2 E[|A_k|^2]}{E[|D_k|^2] + E[|W_k|^2]} \\ &= \frac{\alpha^2 P_{in,k}}{P_{d,k} + \frac{P_{noise}}{N}} \end{aligned} \tag{37}$$

of which the inverse is

$$\begin{aligned} \mathrm{SNDR}_k^{-1} &= \frac{P_{d,k}}{\alpha^2 P_{in,k}} + \frac{P_{noise}}{\alpha^2 N P_{in,k}} \\ &= \mathrm{SDR}_k^{-1} + \mathrm{SNR}_c^{-1} \frac{\beta P_{out}}{\alpha^2 N P_{in,k}} \end{aligned} \tag{38}$$

$$C = \frac{1}{N} \sum_{P_{in,k}=P_{in}}^{\max} \sum_{k=0}^{N-1} C_k$$

$$= \frac{1}{N} \sum_{P_{in,k}=P_{in}}^{\max} \sum_{k=0}^{N-1} \log_2 (1 + \mathrm{SNDR}_k) \quad \text{bits/subcarrier} \tag{39}$$

Since the received signal can be modeled as a sum of a linearly attenuated signal and the Gaussian noise plus Gaussian distortion, without any constraint on the input signal except the average input power P_{in}, the average channel capacity *per subcarrier* (i.e., per complex dimension) will be given by (39), Equation (39) could be maximized via the water-filling principle Since $P_{d,k}$ is a0 function of all the $P_{in.k}$, it appears that the solution that maximizes (39) may not be given in a simple closed form. In [85, Ch. 7], the maximization is performed by the iterative algorithm and it is shown that the gain in channel capacity achieved by the water-filling is practically negligible, compared to the case with the equally distributed allocation of the input power.

Thus, in what follows, we assume that the input power of each subcarrier is equally distributed for simplicity. The capacity (39) then reduces to

$$C = \frac{1}{N} \sum_{k=0}^{N-1} \log_2 (1+\mathrm{SNDR}_k) \text{ bits/subcarrier.} \tag{40}$$

The inverse of SNDR_k is now given by

$$\mathrm{SNDR}_k^{-1} = \mathrm{SDR}_k^{-1} + B \tag{41}$$

where B is a constant expressed as

$$B = \mathrm{SNR}_c^{-1} \frac{\beta}{K\gamma} = \mathrm{SNR}_c^{-1} \left\{ 1 + \frac{1}{N} \sum_{k=0}^{N-1} \mathrm{SDR}_k^{-1} \right\} \tag{42}$$

due to the constraint that the power allocation of each subcarrier is equal, i.e., $P_{in,k} = P_{in}/N$ for all k. Equation (40) is a function of the SNR and the SDR_k which can be calculated from (D19) in the Appendix.

In the case of the Nyquist-rate clipping (the clipping without oversampling), i.e., $J = 1$, the distortion term is equally distributed within the entire bandwidth and the SDR_k can be given in the following closed-form expression [60]:

$$SDR_k = \frac{K\gamma}{1 - K\gamma}, \text{ for } k = 0,1,\ldots, N\ 1 \tag{43}$$

and thus (41) further reduces to [60]

$$SNDR^{-1} \equiv SNDR_k^{-1} = \frac{1 - K\gamma + SNR_c^{-1}}{K\gamma} \tag{44}$$

Therefore in this case the channel capacity is given by

$$C = \log_2 (1 + SNDR)$$

$$= \log_2 \left(\frac{1 + SNR_c^{-1}}{1 - K\gamma + SNR_c^{-1}} \right) \text{ bits/subcarrier} \tag{45}$$

6.2.2. *Channel Capacity over a Rayleigh Fading Channel*

With an ideal interleaving of the channel, the received signal at the decoder can be expressed from (22) and (28) as

$$\hat{A}_k = H(\alpha A_k + D_k) + W_k = H(\alpha A_k) + Z_k^I \tag{46}$$

where $Z_k^I \triangleq HD_k + W_k$. Again, we assume that the input power of the subcarrier is equally distributed and Z^1_k is an additive Gaussian noise independent of the input signal. With ideal symbol-wise interleaving and perfect CSI, the channel capacity over a Rayleigh fading channel is given by [84, p. 361]

$$C = E[C(H)] = \int_0^\infty C(H) f(H) dH \tag{47}$$

Where

$$C(H) = \frac{1}{N} \sum_{k=0}^{N-1} \log_2 (1 + SNDR_k(H)) \tag{48}$$

and $f(H) = 2Hc^{-H^2}$ is a Rayleigh probability density function(pdf) normalized such that $E[H^2] = 1$. The SNDR of the k^{th} subcarrier is given as a function of H by

$$\mathrm{SNDR_k(H)} = \frac{E[|H\alpha A_k|^2]}{E[|HD_k + W_k|^2]}$$

$$= \frac{E[|H\alpha A_k|^2]}{E[|HD_k|^2] + E[|W_k|^2]}$$

$$= \frac{H^2\alpha^2 P_{in,k}}{H^2 P_{d,k} + \mathrm{P_{noise}}/N} \tag{49}$$

of which the inverse is

$$\mathrm{SNDR_k}(H)^{-1} = \frac{P_{d,k}}{\alpha^2 P_{in,k}} + \frac{P_{noise}}{H^2\alpha^2 N P_{in,k}}$$

$$= \mathrm{SDR_k^{-1}} + \mathrm{SNR_c^{-1}} \frac{\beta P_{out}}{H^2\alpha^2 N P_{in,k}} \tag{50}$$

Here, $\mathrm{SNR_c}$ corresponds to the *average* channel SNR. Since the power allocation of each subcarrier is assumed equal, (50) reduces to

$$\mathrm{SNDR_k}(H)^{-1} = \mathrm{SDR_k^{-1}} + \frac{1}{H^2} B \tag{51}$$

Carrying out the integration of (47) yields

$$C = \frac{1}{(1n2)N} \sum_{k=0}^{N-1} \left\{ e^{B/(\mathrm{SDR_k^{-1}}+1)} \mathrm{E1}\left(\frac{\mathrm{B}}{\mathrm{SDR_k^{-1}}+1.}\right) - e^{BSDR_k} E_1(BSDR_k) \right\} \tag{52}$$

where $E_n(x)$ is the exponential integral defined as

$$E_n(x) = \int_1^\infty \frac{e^{-xt}}{t^n} dt \qquad x > 0 \tag{53}$$

In the case of the Nyquist-rate clipping, (52) reduces to

$$C = \frac{1}{\ln 2}\left\{ e^{1/(SNR_c)} E1\left(\frac{1}{SNR_c}\right) - e^{1/((1-k\gamma)SNR_c)} E1\left(\frac{1}{(1-K\gamma)SNR_c}\right)\right\} \quad (54)$$

6.2.3. *Channel Capacity with Input Constraint*

It is of practical interest to investigate the channel capacity when the input has a constraint on the signal constellation. In the following, It is consider the rectangular M-ary quadrature amplitude modulation (M -QAM) (or QPSK when M = 4). The additive noise terms Z^1_k are assumed to be Gaussian, independent of the input signal (i.e., the worst-case bound). The conditional average mutual information given the channel coefficient H is then expressed as

$$C = \frac{1}{N}\sum_{k=0}^{N-1} I(A_k, \tilde{A}_k|H)$$

$$= \frac{1}{N}\sum_{k=0}^{N-1}\left\{ h(A_k|H) - h(A_k|\tilde{A}_k, H)\right\} \quad (55)$$

where $h(X|Y)$ is the conditional differential entropy of X given Y. For M-QAM, the conditional average mutual information is given by

$$I(A_k, \tilde{A}_k|H) = \log_2 M - E\left[\log_2 \frac{1}{f(A_k|\tilde{A}_k, H)}\right] \quad (56)$$

where the expectation is over A_k, $\tilde{A}_k$, and also H for a fading channel and $f(X|Y)$ is the conditional pdf of X given Y. Let the S_i, i =1, 2,...M, denote the complex-valued constellation of the input signal A_k and assume that all the input constellations are equally probable. In equation (57) $f(\tilde{A}_k|A_k = S_i, H)$ is a two-dimensional Gaussian pdf centered at S_i with variance given by $E[|A_k|^2]\mathrm{SNDR}_k(H)^{-1}$

$$E\left[\log_2 \frac{1}{f(A_k|\tilde{A}_k, H)}\right] = \sum_{i=1}^{M}\int_0^\infty \int_{-\infty}^{\infty} f(A_k = S_i, \tilde{A}_k, H)\log_2 \frac{1}{f(A_k = S_i|\tilde{A}_k, H)}\, d\tilde{A}_k dH$$

$$= \frac{1}{M}\sum_{i=1}^{M}\int_0^\infty f(H)\int_{-\infty}^{\infty} f(\tilde{A}_k|A_k = S_i, H)\log_2 \frac{\sum_{i=1}^{M} f(\tilde{A}_k|A_k = S_i, H)}{f(\tilde{A}_k|A_k = S_i, H)}\, d\tilde{A}_k dH \quad (57)$$

Unfortunately, a closed form or convenient expression for numerical calculation has not been found for the above equation and thus It is resort to the Monte Carlo method [94]. It is now show the channel capacity of the clipped OFDM signals for various parameters of particular interest. In the calculation, the following three cases are considered: the channel capacity without input constraint (i.e., Gaussian input), with QPSK, and rectangular 16-QAM inputs. The number of subcarriers is assumed to be 512, but this number may not show noticeable difference in terms of channel capacity, as long as Gaussian approximation of the OFDM signals holds.

6.2.4. *Channel Capacity without Input Constraint*

The paper[96] shows the channel capacity of the clipped OFDM signals without input constraint over AWGN and ideally interleaved Rayleigh fading channels. It is observed that the clipping severely bounds the achievable channel capacity. For example, for the case of the hard-envelope limiter ($\gamma = 0$), the figure indicates that it is not theoretically possible to achieve error-free performance with an information data rate of 3 bits per subcarrier.

6.2.5. *Channel Capacity with Input Constraint and Required Channel SNR*

Also it[96] shows that the channel capacity when each subcarrier is modulated by QPSK and 16-QAM, respectively, with $\gamma = 0$ and 1.0. It clearly shows that with $\gamma = 0$ and QPSK signaling it is impossible to achieve error-free performance of information data rate 2 bits per subcarrier, no matter how much one may increase the channel SNR. Nevertheless, the figure also indicates that the capacity of 1 bit per subcarrier can be achieved with QPSK and optimal rate 1/2 channel coding.

The question is how much the degradation would become in terms of the required channel SNR for a given targeted channel capacity. The required channel SNR in order to achieve an information data rate of 1 bit per subcarrier with QPSK signaling is shown with respect to the

clipping ratio γ.It is observed that, with , the $\gamma = 0$ increase in the required channel SNR is within 1.5 dB for $J = 16$, while it becomes more than 2.5 dB for $J = 1$.

It is concluded that, for QPSK signaling, the distortion may not lead to severe performance degradation, provided that a good channel coding is employed; however, the clipping ratio should be carefully chosen if one uses a signaling of higher order such as 16- QAM for higher bandwidth efficiency, since the performance becomes much more sensitive as the clipping ratio decreases, even with optimal channel coding.

6.2.6. *BER Evaluation*

It is further justified the argument of channel capacity with the help of near optimal turbo codes [80]. The parameters chosen are as follows. The numbers of subcarriers are 512 and each subcarrier is modulated by QPSK. Thus, each OFDM symbol is able to carry 1024 bits. The interleaver size of the turbo codes is 16378 and both the trellises of the two identical component convolutional codes, each having memory of 4, are terminated and each parity bit of the convolutional code is punctured such that the overall coding rate is approximately 1/2 [80].Consequently, the total length of the code word is $TL = 2 \times 16378 + 4 \times 3 = 32768$ and the coding rate is $R = 16378/TL \approx 1/2$. The code word is divided into 32 sets of length 1024 and each set is transmitted as one OFDM symbol with 512 subcarriers. At the decoder, the distortion is treated simply as an additive Gaussian noise. The maximum *a posteriori* (MAP) decoding based on the BCJR algorithm [38] requires the knowledge of the variance of the additive noise .It is assumed that the decoder has the knowledge of the variance averaged over all the subcarriers.

The bit-error performance of the turbo codes over an ideal channel is within 1 dB of the channel capacity at bit error rate (BER) 10^{-5} . The figure below show the performance within 1 dB of the corresponding channel capacity at BER 10^{-5}.

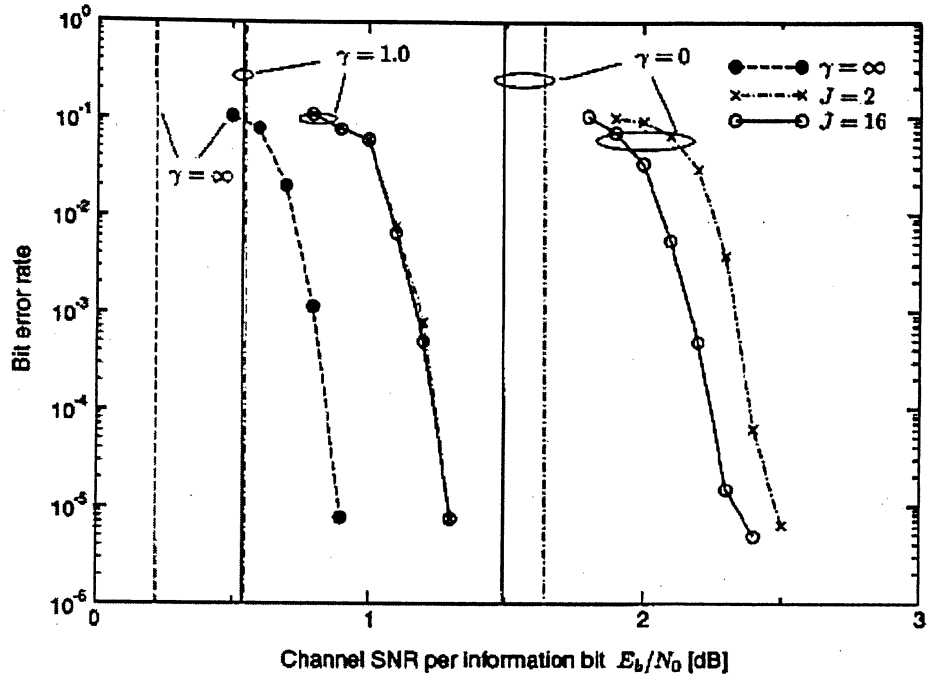

Fig. 6-1. BER performance of the clipped OFDM systems with turbo codes. The vertical lines indicate the required minimum channel SNR values in order to achieve the corresponding channel capacity. [96]

7. RADIO OVER FIBER TRANSMISSION

The waveforms of the optical pulses are influenced by attenuation, dispersion and nonlinear effect. In the RoF-OFDM [95] system because of short distance of fiber, the major concerning factors are dispersion and nonlinear effect. Gaussian pulses are generated by laser propagate in the optical fibers along the z axis; the variety of the intensity can be described by Schrödinger equation [92], [93]:

$$\frac{\partial A}{\partial z}+\frac{\alpha}{2}A+\beta_1\frac{\partial A}{\partial t}+\frac{1}{2}\beta_2\frac{\partial^2 A}{\partial t^2}-\frac{1}{6}\beta_3\frac{\partial^3 A}{\partial t^3}=i\gamma|A|^2A \tag{1}$$

Where, i denote the imaginary unit. A(z,T) denotes the amplitude of optical pulses, z is the fiber length, T is the time parameter based on the reference system of group velocity of the central wavelength. $\gamma=n_2w_0/cA_{\text{eff}}$ is the nonlinear coefficient; A_{eff} is the effective mode area. In the following analysis, assume $A(z,T)$ is the normalized amplitude.

According to the Split-step Fourier Method,[93] It is obtained

$$\frac{\partial A}{\partial T}=(D+N)A \tag{2}$$

Where, $\hat{D}$ is the differential function that represents the dispersion and $\hat{N}$ absorption of linear medium, and in the nonlinear function:

$$\hat{D}=-\frac{1}{2}\beta_2\frac{\partial}{\partial T^2}+\frac{1}{6}\beta_3\frac{\partial^3}{\partial T^3}-\frac{\alpha}{2} \tag{3}$$

$$\hat{N}=i\gamma|A|^2 \tag{4}$$

The Split-step Fourier Method divides the fiber to many parts. Assume the total length of the fiber is L, for each part, the length is h. The dispersion and nonlinear effect can be considered separately in the small part. That is, from z to z+h, first consider the nonlinear effect, and ignore the dispersion and loss, so in (2), $\hat{D}$ = 0; then, consider the dispersion and loss only, which means $\hat{N}$ = 0 in (2). So it is obtained as:

$$A(z+h,T) \approx \exp(h\hat{D}) \exp(h\hat{N})\, A\,(z,T) \tag{5}$$

For exp ($h\hat{D}$) in the Fourier domain:

$$\exp(h\hat{D})U(z,T) = F_T^{-1} \exp[h\hat{D}(i\omega)]A(z,T)F_T\{U(z,T)\} \tag{6}$$

Where F_T is Fourier transform; $\hat{D}$ (iω) is obtained from (4) that represents the differential coefficient $\partial / \partial T$ with $i\omega$, ω is the frequency in the Fourier Domain. With the Fast Fourier Transform Method, it is faster to solve(6)

7.1 Optical Transmission Performances of OFDM-64QAM

The figure 7-2 shows the measurement and calculation results of the OFDM-64QAM [57].It shows the measurement and calculation results of the carrier-to-noise ratio (CNR), ACLR, and relative constellation error versus the OMI in the downlink where the optical received Power is Pr = -2.6 dBm. The CNR is calculated by

$$\mathrm{CNR}(m,Pr) = 10\log\left[\frac{(m\cdot\eta\cdot Pr/\alpha)^2 Zo/2}{(RIN\cdot(\eta\cdot Pr/\alpha)^2 + 2q\cdot\eta\cdot Pr + In^2)\cdot B\cdot Zo}\right] \tag{1}$$

$$m = m_e/\beta$$

where m is the OMI, m_e is the electrical modulation index of the input signal to LD, ∝ = 5dB is the relative loss of the PD at the signal frequency, β = dB is the relative loss of the LD at the signal frequency, Pr is the optical received power, η = 0.9A/W is the photodiode responsivity, RIN = -150dB/Hz is the relative intensity noise of the LD, q is the electron charge, In = 12 pA / $\sqrt{\text{Hz}}$ is the total equivalent input current noise of the preamplifier with the PD,B = 18 MHz is the signal bandwidth, and Z_0 is the characteristic impedance.

As the figure 7-1 shows, all the requirements for CNR, ACLR, and the relative constellation error are satisfied in the OMI range from 3.5% to 30%. In addition, the minimum optical received power, which is the minimum limit of optical received power satisfying both the required relative constellation error and CNR, is -14 dBm. The results of the ACLR and CNR are used in this study

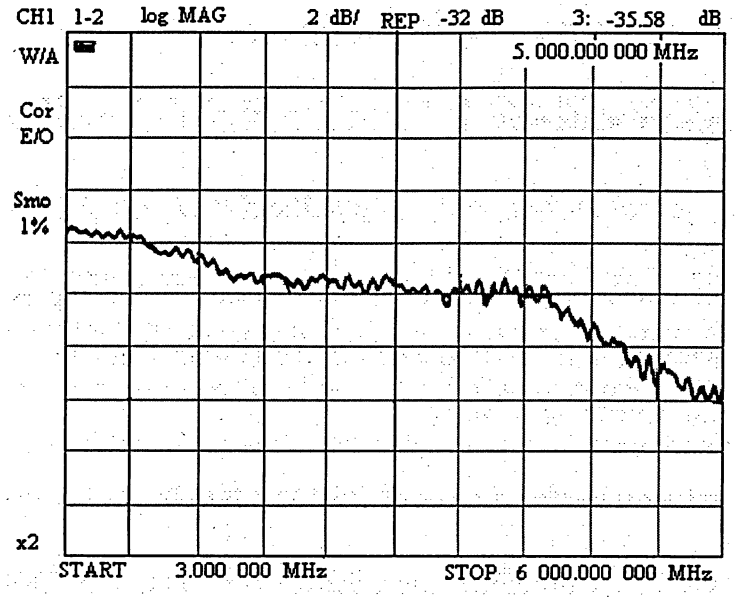

(a)

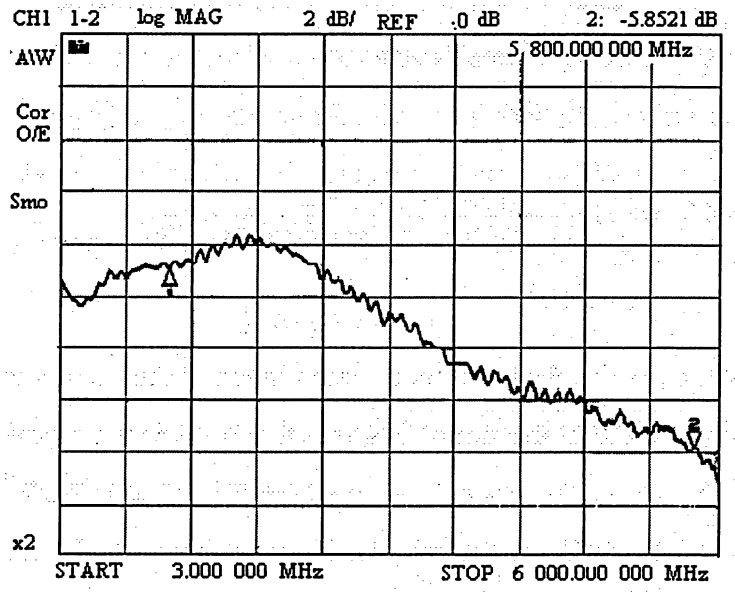

(b)

Fig.7-1. Frequency responses of narrow-band DFB LD and p-i-n PD used in the experiments. (a) DFB LD. (b) p-i-n PD (in this figure, START freq.: 3 MHz, STOP freq.: 6 GHz, v-axis: 2 dB/div).[97]

TABLE II :Main characteristics of narrow-band DFB LD and of PIN PD

DFB-LD	
Wavelength	1.55μm
Relative Intensity Noise	-150dB/Hz
The output powder of the third order intercept point (@optical received power – 0dBm	-14 dBm
Optical output power (@bias current -55mA)	4.5 mW
Threshold current	12 mA
p-i-n PD	
Responsivity	0.9 A/W

Fig. 7-2(b) shows the measurement results of the PER and relative constellation error versus the OMI in the uplink where the packet size in the PER measurement is 1023 octets.[97]

As shown in this figure, the required PER of less than 0.1 is satisfied in the OMI range from 0.42% to 30%. This OMI range corresponds to a dynamic range of 37 dB, which satisfies the 35-dB specification.

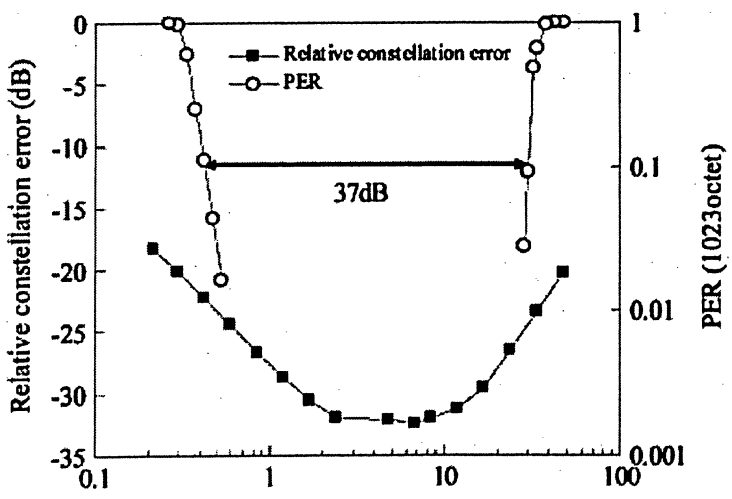

OMI (%)

(a)

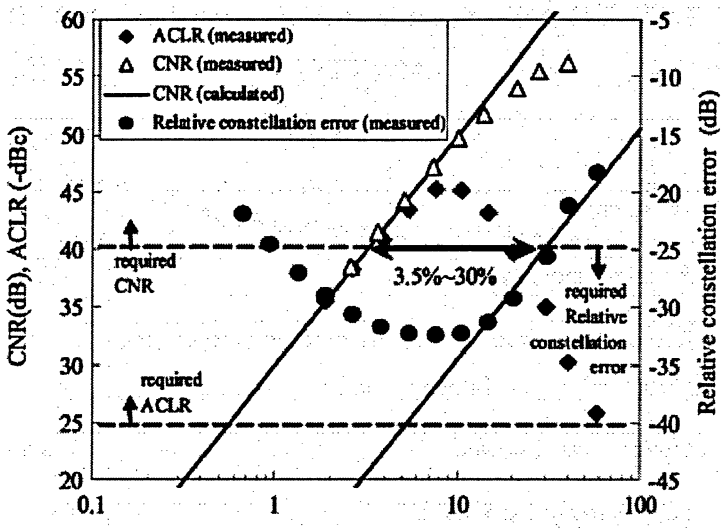

(b)

Fig. 7-3. Measurement characteristics of OFDM-64QAM. (a) ACLR, CNR, and relative constellation error in downlink. (b) Relative constellation error and PER in uplink. [97]

7.2 Optical Transmission Performances of COMPLIMENTARY CODE KEYING (CCK)

Fig. 7-4 shows the measurement results for CCK. Fig. 7-4(a) shows the measurement results of the spectral products and the EVM in the downlink, where the spectral products are the peak powers of the sidelobe in the frequency ranges: 1) from f_c + 11 MHz to f_c + 22 MHz, where f_c is the center frequency of the modulated signal and 2) higher than f_c + 22MHz.

As shown in Fig. 7-4(a), the requirements for transmitting spectral mask and the EVM are satisfied under the following OMI conditions.

1) In the OMI from 6.1% to 80%, the required transmit spectrum mask of less than -50 dBc, which is specified from f_c + 11 MHz to f_c + 22 MHz,is satisfied.

2) In the OMI from 0.62% to 101.5%, the required transmit spectrum mask of less than -30 dBc, which is specified in the frequency of higher than f_c + 22 MHz, is satisfied.

3) In OMIs of more than 0.1%, the required EVM of less than 35% is satisfied.

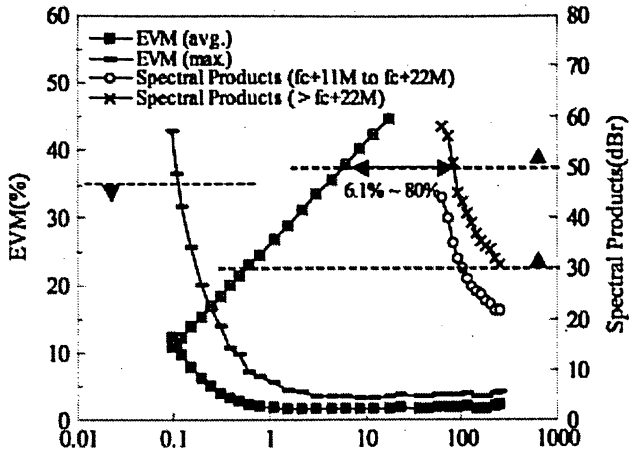

(a)

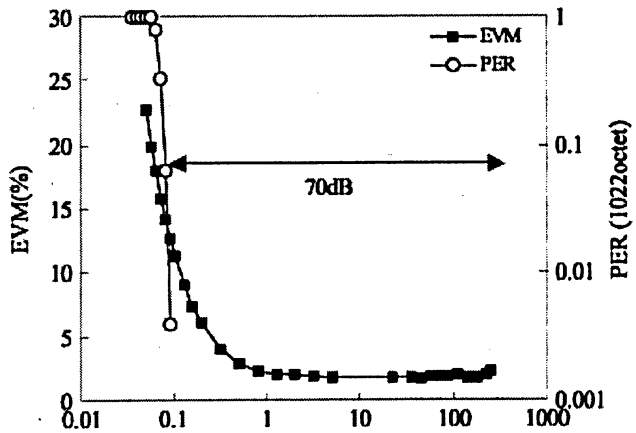

(b)

Fig. 7-4 Measurement characteristics of CCK. (a) Spectral products and EVM in downlink. (b) EVM and PER in uplink.[97]

From these OMI ranges, all requirements for the downlink are satisfied in the OMI ranges of 6.1%–80%.

Fig. 7-4(b) shows the measurement results of the PER and EVM versus the OMI in the uplink where the packet size in the PER measurement is 1022 octets. As shown in the figure, the required PER of less than 0.08 is satisfied under the OMI of more than 0.08%. This OMI range corresponds to a dynamic range of more than 70 dB, which satisfies the 66-dB specifications.

In the lower range of the OMI, both the spectral products and EVM are dominated by noise. In the higher range of the OMI, although the spectral products are degraded by nonlinear distortion of the DFB LD, the EVM is not degraded. This is attributed to the fact that the CCK scheme is phase modulated and the signal amplitude does not have any role in transmitting data.

7.3 Optical Transmission performances of Multichannel WLAN signals

Here, it is evaluated the optical transmission performances of multichannel WLAN signals using the measurement results [97] of the single-channel transmission.

Firstly, It is presented the analysis method of multichannel transmission performances taking into consideration the spectral distribution of a modulated signal. Next, the analysis method is validated with the measurements of the dynamic range in the optical transmission of four-channel WLAN signals. Finally, the dynamic ranges of up to seven-channel WLAN signals are calculated in both the uplink and downlink. In addition, the cell size and minimum optical received power are estimated in the uplink and downlink, respectively.

7.3.1 Composite Distortion

In the optical transmission of multichannel signals, nonlinearity of an LD creates composite distortion products that have a great impact transmission quality, especially on the desired-to undesired signal power ratio (DUR). In a multichannel WLAN system, the composite distortion products should be evaluated while taking into consideration the spectral distribution of a modulated signal because these signals cause the spectral broadening of a third-order distortion, which then degrades the signal qualities in adjacent channels. In addition, second-order distortion products are out-of-band because the transmission bands are from 2400 to 2483.5 MHz and from 5150 to 5250 MHz. Therefore, It is concentrate on third-order distortion products.

It is now introduce the analysis method of third-order distortion products into the evaluation of multichannel transmission performances. In the analysis, It is calculate the composite third-order distortions for modulated signals. Specifically, the spectral distribution of a modulated signal is incorporated into the conventional calculation method of the composite triple beats (CTB) for unmodulated carriers.

Fig.7-5 shows diagrams of the analysis method. As shown in Fig. 7-5(a), the CTB created by the optical transmission of multi-tone unmodulated carriers are calculated. As shown in Fig. 7-5(b), the spectral distribution of a third-order distortion created by a modulated signal transmission is calculated. By using the calculation results of both the CTB and the spectral distribution, the composite third-order distortions in the desired signal channel are calculated as shown in Fig. 7-5(c).

Firstly, it is assume that the input signal to an RoF link v_{in} consists of N unmodulated carriers

$$\upsilon_{in} = \sum_{n=1.}^{N} a_n \cos(2\pi f n t + \varphi n) \tag{2}$$

where a_n is the peak amplitude at frequency f_n. The transfer function of a RoF link can be modeled by a Taylor-series expansion

$$\upsilon_{out} = K_0 + K_1 \upsilon_{in} + K_2 \upsilon_{in}^2 + K^3 \upsilon_{in}^3 + \ldots \tag{3}$$

where v_{out} is the output signal of a RoF link and K_n is an nth-order coefficients.

The relative amplitude of third-order inter-modulation to carrier is calculated on the assumption that the phase of each accumulated beat is random as follows:

$$d(f_n) = \sqrt{\sum_{i,j,k} \left(\frac{1}{4} K_3 a_i a_j a_k\right)^2} \Big/ K_1 a_n$$

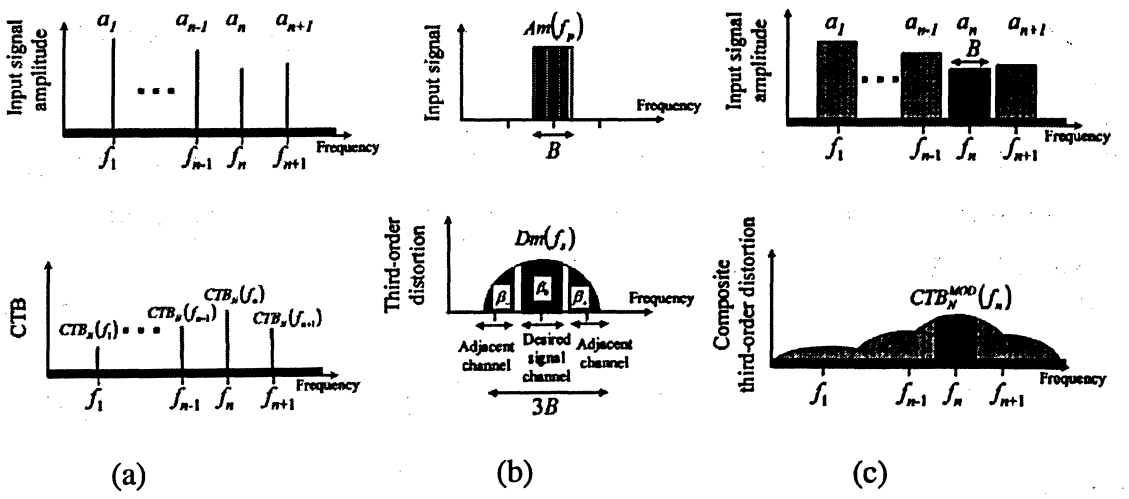

Fig. 7-5. [97] Calculation method for composite third-order distortion products of multichannel modulated signals. (a) CTBs from multitone carriers are calculated. (b) Spectral distribution of a third-order distortion from a modulated signal is calculated. (c) From (a) and (b), composite third-order distortion products of multichannel modulated signals are calculated.

$$= \frac{1}{4}\frac{K_3}{K_1} a_{max}^2 \sqrt{\sum_{i,j,k} (\Delta a_i \Delta a_j \Delta a_k)^2 \Delta a_n} \quad (4)$$

where $a_n \equiv a_{max}\ \Delta\ a_n$, a_{max} is the maximum amplitude among input carriers, a_n is the signal amplitude of the input carrier at number n, Δa_n is the relative amplitude of to a_{max} and i,j,k are the number of input carriers that satisfy $f_i \pm f_i \pm f_k = f_n$. Thus, the CTB generated by the unmodulated carriers at a frequency of f_n is given by

$$\begin{aligned} CTB_N(f_n,m) &= 10 \log [d(f_n)^2] \\ &= IM3_{max} + 10 \log [C_N(f_n, m)] - 20 \log(\Delta a_n) \end{aligned} \quad (5)$$

where

$$m = \{m_1,\ldots m_{n-1}, m_n, m_{n+1},\ldots,m_n\}$$

$$IM3_{max} = 20 \log \left[\frac{3}{4}\frac{K_3}{K_1} a_{max}^2\right]$$

$$\begin{aligned} C_N(f_n,m) &= \frac{1}{9}\sum_{i,j,k} (\Delta a_i \Delta a_j \Delta a_k)^2 \\ &= \frac{1}{9}\sum_{i,j,k} \left(\frac{m_i m_i m_k}{m_{max}^3}\right)^2 \end{aligned}$$

$IM3_{max}$ is a third-order intermodulation of two-tone carriers with an amplitude of a_{max}, $C_N(f_n,m)$ is a composite number taking into consideration the amplitude of each unmodulated carrier, m_n is the OMI of he input carrier at number n, and m_{max} is the maximum OMI among input carriers.

Next, It is to calculate the spectral distribution of a third-order distortion, which is created by the transmission of a modulated signal. The Fourier-series expansion of a modulated signal with bandwidth B is

$$v_{sig} = \sum_{p=-M/2}^{M/2} am_p \cos(2\pi f_p t) \quad (6)$$

where $am_p = \sqrt{Am(f_p)\cdot\Delta f}$, $\Delta f = f_p - f_{p-1} = B/M$ am_p is the amplitude of the elementary component at frequency f_p,$Am(f_p)$ is the spectral distribution of the modulated signal, and M is the number of elementary components. The third-order distortion has three times the bandwidth of a modulated signal, and it is expressed as

$$v_{3dis} = \sum_{s=-3M/2}^{3M/2} dm_s \cos(2\pi f_s t) \tag{7}$$

where $dm_s = \sqrt{Dm(fs)\cdot\Delta f}$, $\Delta f = f_s - f_{s-1} = B/M$, dm_s is the amplitude of the elementary component at frequency f_p, and $Dm(f_s)$ is the spectral distribution of the third-order distortion. The elementary components of third-order distortion are the intermodulation products with respect to each elementary component of the modulated signal. Thus, the amplitude of the third-order distortion of the elementary component dm_s is calculated in the same way as (4), i.e

$$\begin{aligned} dm_s &= \sqrt{\sum_{p,q,r} \left(\frac{1}{4} K_3 \cdot am_p \cdot am_q \cdot am_r\right)^2} \\ &= \frac{1}{4} K_3 \sqrt{\sum_{p,q,r} Am(f_p)\cdot Am(f_q)\cdot Am(f_r)\cdot \Delta f^3} \end{aligned} \tag{8}$$

$$dm_s = \frac{1}{4} K_3 \sqrt{\sum_{p=-M/2}^{M/2} \sum_{q=-M/2}^{M/2} Am(f_p)\cdot Am(f_q)\cdot Am(f_s - f_p + f_q)\cdot \Delta f^3} \tag{9}$$

$$Dm(f_s) = \left[\frac{1}{4} K_3 \sqrt{\int_{-B/2}^{B/2}\int_{-B/2}^{B/2} Am(f_p)\cdot Am(f_q)\cdot Am(f_s - f_p + f_q)\, df_p\, df_q}\right]^2 \tag{10}$$

By substituting $f_s = f_p + f_q + f_r$ into (8), the amplitude dm_s is (9), shown at the bottom of the following page. In order to obtain the spectral distribution of the third-order distortion $Dm(f_s)$ the frequency spaces of each elementary component is converged to zero ($\Delta f \to 0$, $M \to \infty$), as shown in (10) at the bottom of the following page.

The power ratio of distortion in the desired signal channel to the total distortion is calculated by

$$\beta_0 = \int_{-B/2}^{B/2} Dm(f_s)\, df_s \Big/ \int_{-3B/2}^{3B/2} Dm(f_s)\, df_s \tag{11a}$$

The power ratio of distortion in an adjacent channel to the total distortion is calculated by

$$\beta_+ = \int_{f_{n+1}-f_n-B/2}^{f_{n+1}-f_n+B/2} Dm(f_s)\,df_s \Big/ \int_{-3B/2}^{3B/2} Dm(f_s)\,df_s \tag{11b}$$

$$\beta_- = \int_{f_{n-1}-f_n-B/2}^{f_{n-1}-f_n+B/2} Dm(f_s)\,df_s \Big/ \int_{-3B/2}^{3B/2} Dm(f_s)\,df_s. \tag{11c}$$

If the spectral distribution of the modulated signal $Am(f_p)$ is constant for in-band and is zero for out-of-band, (11a)–(11c) can be simply expressed as

$$\begin{aligned}\beta_0 &= \frac{2}{3}\\ \beta_+ &= \frac{1}{6}\left(2 - \frac{f_{n+1}-f_n}{B}\right)^3\\ \beta_- &= \frac{1}{6}\left(2 - \frac{f_n - f_{n-1}}{B}\right)^3.\end{aligned} \tag{12}$$

It is then to calculate the third-order distortions in a multichannel transmission of modulated signal using (5) and (12). By modulating the carriers, the spectrum of the CTB $CTB_N(f_n,m)$, in which power is concentrated at a frequency of f_n, is broadened over the adjacent channels. The composite third-order distortions in the desired signal channel, which are created by modulated signals, are the summation of both the composite third-order distortions centered at the desired signal channel $\beta_0 \cdot d(f_n)^2$ and the leakage of the composite third-order distortions centered at adjacent channels $\beta_- \cdot d(f_{n+1})^2$ and $\beta_+ \cdot d(f_{n-1})^2$. Thus, the relative power of the composite third-order distortion in the desired signal channel is given as

$$\begin{aligned}&CTB_N^{MOD}(f_n, m)\\ &\quad = 10\log\left[\beta_0 \cdot d(f_n)^2 + \beta_- \cdot d(f_{n+1})^2 + \beta_+ \cdot d(f_{n-1})^2\right]\\ &\quad = IM3_{max} + 10\log\left[C_N^{MOD}(f_{n+1}, m)\right] - 20\log(\Delta a_n)\end{aligned} \tag{13}$$

where

$$C_N^{MOD}(f_n,m) = \beta_0 \cdot C_N(f_n,m) + \beta_- \cdot C_N(f_{n+1},m) + \beta_+ \cdot C_N(f_{n-1},m)$$

f_n is the center frequency of the desired channel, is the f_{n+1} is the center frequency of the higher adjacent channel, and is f_{n-1} is the center frequency of the lower adjacent channel.

The DUR for the desired channel is

$DUR_N(f_n,m)$

$$= 10\log\left[10^{\frac{-CTB_N^{MOD}(f_n,m)}{10}} + 10^{\frac{CNR(f_n)}{10}}\right]$$

$$= 10\log\left\{\Delta a_n^2 / \left[10^{\frac{IM3_{max}}{10}} \cdot C_N^{MOD}(f_n,m) + 10^{-\frac{CNR_{max}}{10}}\right]\right\}$$

$$= 20\log\left(\frac{m_n}{m_{max}}\right) - 10\log\left\{10^{\frac{IM3_{max}}{10}} \cdot C_N^{MOD}(f_n,m) + 10^{-\frac{CNR_{max}}{10}}\right\} \quad (14)$$

where

$$CNR(f_n) = CNR_{max} + 20\log(\Delta a_n)$$

m_n is the OMI of the desired signal and m_{max} is the maximum OMI among input signals. $IM3_{max}$ and CNR_{max} are calculated by the measured performances of a single-channel transmission

$$IM3_{max} = ACLR_{measure} - 10\log(\beta_{adj}) + 40\log(m_{max}/m_{measure}) \quad (15)$$

$$CNR_{max} = CNR_{measure} + 20\log(m_{max} / m_{measure}) \quad (16)$$

where $\beta_{adj} \equiv \beta_+ = \beta_-$ assuming that the channel space f_{n+1} f_n of and channel space of f_n f_n are the same, $ACLR_{measure}$ and $CNR_{measure}$ and are the measured ACLR and CNR at the OMI of $m_{measure}$ in a single-channel transmission.

By substituting the measured ACLR and CNR for (15) and (16), the DUR for multichannel WLAN signals can be calculated by (14). Thus, we can estimate the DUR of multichannel transmission only measuring the CNR and ACLR of single channel transmission. Therefore, the analysis method is useful for the practical design of a multichannel WLAN system.

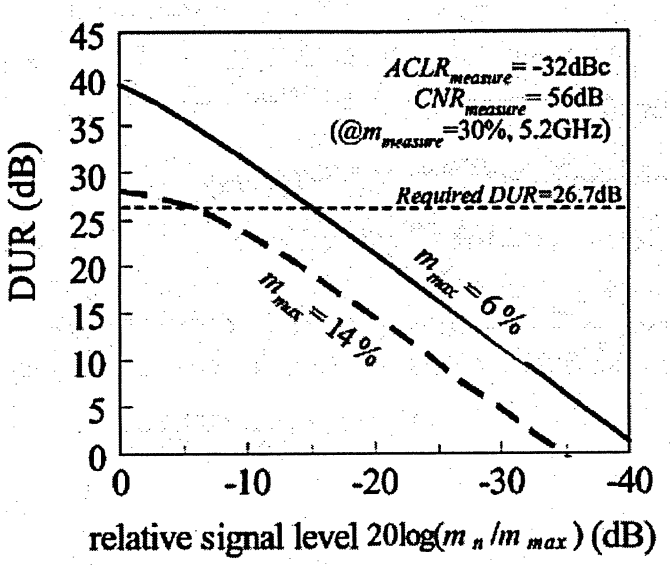

Fig. 7-6. Calculation results of the DUR for the four-channel multiplexed signals in the uplink.

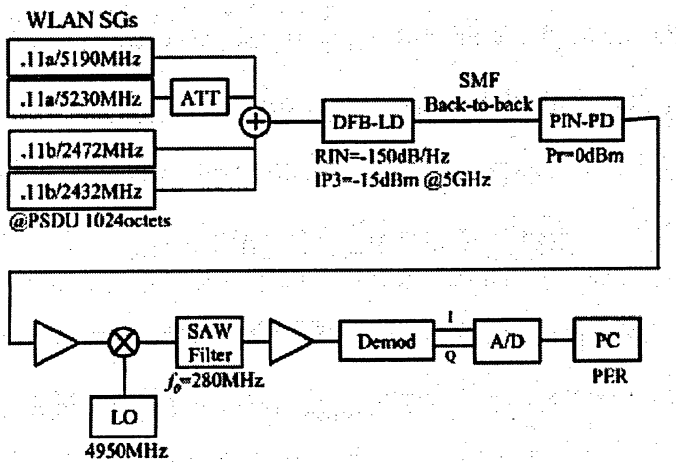

Fig. 7-7. Experimental set up for the measurement of the dynamic range in four-channel WLAN signal transmission.

Fig. 7-6 shows the calculation results of the relative signal level 20 log(m_n / m_{max}) versus the DUR in the optical transmission of four-channel signals. It is calculated using the measured ACLR $ACLR_{measure}$ and the measured CNR $CNR_{measure}$ in the experimental setup shown in Fig. 7-7 while assuming the following conditions.

1) The frequency of each signal is 2432, 2472, 5190, and 5230 MHz.

2) The desired signal frequency f_n is 5230 MHz.

3) These signal levels are set taking into consideration the worst case.

Specifically, the OMI of the undesired signal, which is any signal, except for the desired signal, are fixed at the maximum OMI m_{max}

As Fig. 7-6 shows, the DUR is degraded with both the reduction of the relative signal level, which causes CNR degradation, and the increase of m_{max}, which causes CTB degradation.

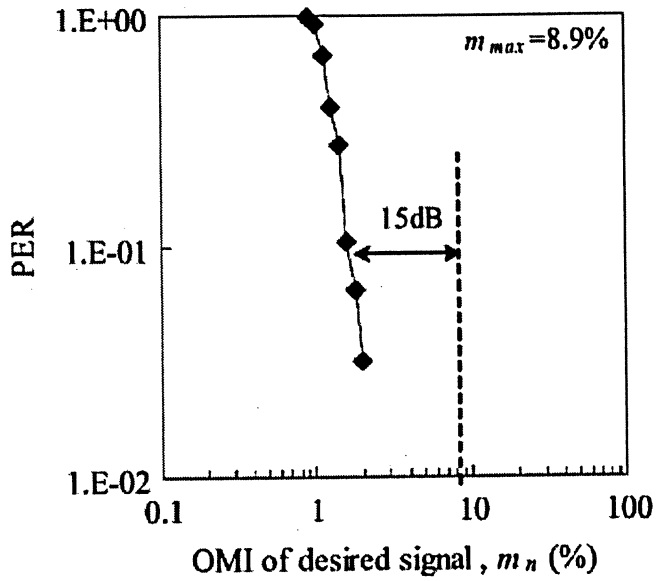

Fig. 7-8. Measurement results of PER versus OMI at m_{max} of 8.9%.

From the calculations of the DUR, the dynamic range for the desired signal is evaluated. The OFDM-64QAM signal, the required DUR that realizes the PER = 0.1, is 26.7 dB. Therefore, the dynamic range is given by the OMI range satisfying that the DUR is more than 26.7 dB as follows:

$$\text{Dynamic Range} = 20 \log [m_n^{MAX}/m_n^{MIN}] \quad (17)$$

where m_n^{max} is the maximum OMI of the desired signal, which corresponds to m_{max}, and m_n^{min} is the minimum OMI of the desired signal, which is the minimum OMI satisfying $DUR_N(f_n,m)$. ≥ 26.7

In this case, the dynamic range is 15.5 dB in the condition of $m_{max} = 6$ %.

7.3.2 Measurement Analysis

To verify the availability of the analysis method[97] outlined above, It is found that the dynamic range of the optical transmission of four-channel WLAN signals. Fig. 7-7 shows the experimental setup. In the experiment, output signals from the p-i-n PD are down-converted to IF signals and the desired signal is then extracted. The four-channel signals are two CCK signals within the frequency of between 2432–2472 MHz, and two OFDM-64QAM signals within the frequency of between 5190–5230 MHz. These signal powers are set taking into

consideration the worst case in the uplink; i.e., the OMI of each undesired signal is fixed at maximum OMI m_{max}

In the experiments, the DUR cannot be measured because the desired signal exists. Therefore, the PER is measured to evaluate the dynamic range. Fig. 7-8 shows the measurement results[97] of the PER versus the OMI of the desired signal m_n when the maximum OMI is set to m_{max} = 8.9%. As shown in this figure, the required PER of less than 0.1 is achieved in an OMI of more than 1.6%. Therefore, the OMI range satisfies the requirements from 1.6% to 8.9%, and it corresponds to the dynamic range of 15 dB.

In a similar way, the dynamic ranges within the conditions of several m_{max} are measured. The measurement and calculated results using the analysis method are shown in Fig. 10, where the dynamic range is calculated by (17). In the calculation, the measured ACLR and CNR in the experimental setup shown in Fig. 8 are used as the value of the parameters of $ACLR_{measure}$ and . The measurement results positively reflect the calculation results. A reminder is that the DUR depends on the maximum OMI m_{max}. In the lower range of m_{max}, the DUR is degraded by noise. In the higher range of m_{max}, the DUR is degraded by composite third-order distortions.

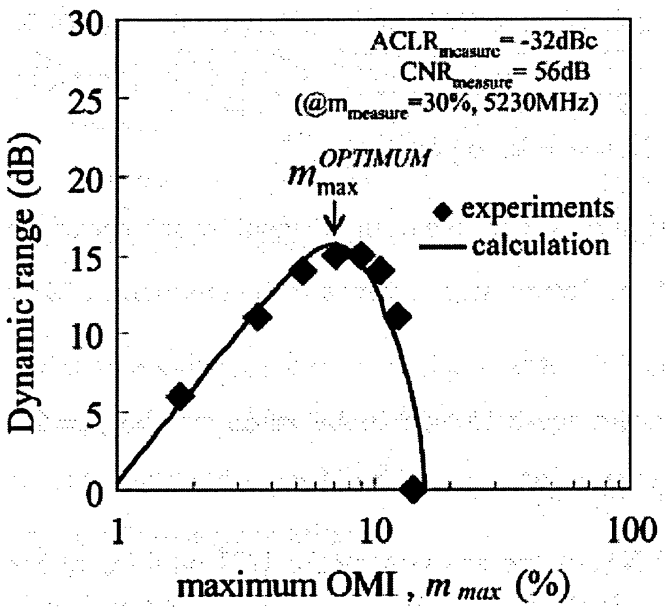

Fig. 7-9. Comparison of measurement results and calculated results in four-channel WLAN signal transmission.

From these results, it is clear that the optimum value of the maximum OMI, which achieves the maximum dynamic range $m_{max}^{OPTIMUM}$, exists. In this case, it is $m_{max}^{OPTIMUM}$%. Therefore,

setting the maximum OMI m_{max} to the optimum value $m_{max}^{OPTIMUM}$ is important to ensure a maximum dynamic range in the uplink. In other words, if the maximum OMI m_{max} is set higher or lower than the optimum value $m_{max}^{OPTIMUM}$, the dynamic range is lowered due to the effects of noise and distortion, respectively.

7.3.3 Evaluation

Using the analysis method, It is found that in optical transmission performances of multichannel WLAN signals, both the uplink and downlink, the dynamic range of the desired signal versus the number of multiplex channels can be calculated using the performances of measured single-channel transmissions. Next, It is evaluate cell size in the uplink and the optical power budget in the downlink. In the analysis, It is focus on the performance of the OFDM-64QAM channel because it requires higher performance than the CCK channel; the cell size and minimum optical received power is also restricted by the performance of the OFDM-64QAM channel.

Fig. 7-10 shows the analysis conditions of this calculation. In the calculation, the performance of the ACLR and CNR shown in Fig. 4 are used as the value of the parameters $ACLR_{measure}$ and $CNR_{measure}$. The transmission performances of both the uplink and downlink are calculated while assuming the following conditions.

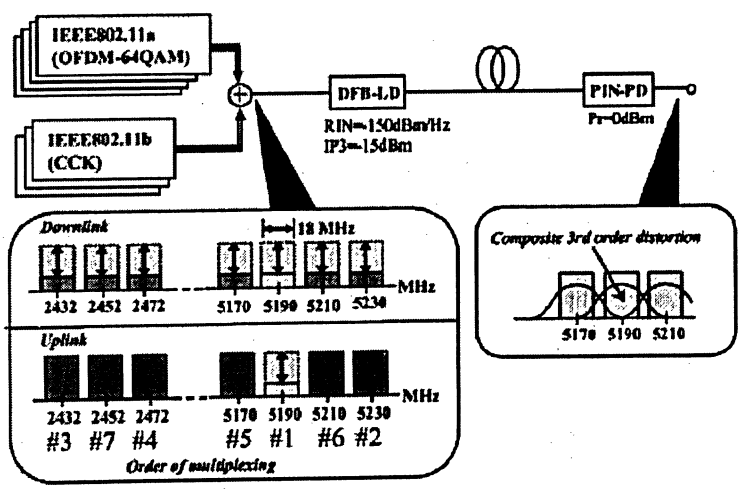

Fig. 7-10 Analysis condition of the multichannel transmission performance in both the uplink and downlink.

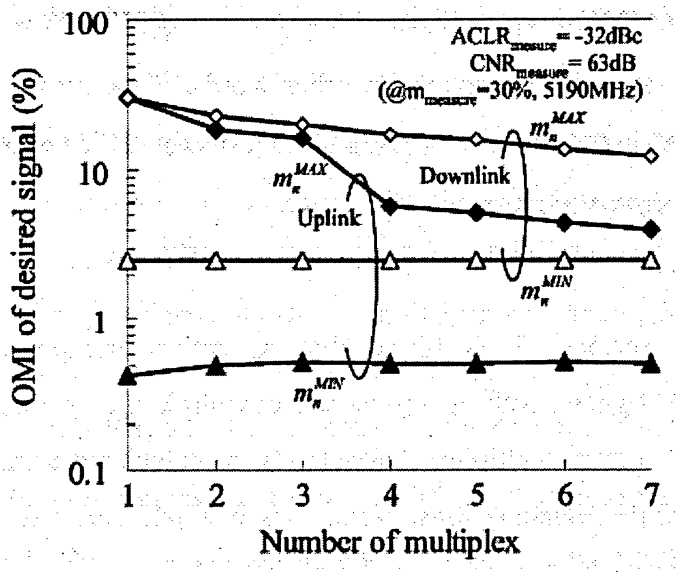

Fig. 7-11. Calculation results of OMI range versus number of multiplex.

1) Input signals are seven-channel WLAN signals that are three CCK signals in the 2.4-GHz band and four OFDM64QAM signals in the 5.2-GHz band.

2) The desired signal frequency is 5190 MHz, which is the 11a-channel.

3) The order of multiplexing is as shown in Fig.7-10 (e.g., in the four-channel transmission, the multiplexed channels are from 1) to 4).

4) The condition of the input multichannel signal is different from the uplink and downlink.

The uplink condition is the worst condition; i.e., the OMI of each undesired signal is fixed at the optimum value of the maximum OMI $m_{max}^{OPTIMUM}$. For the downlink, the OMI of all signals are the same as the OMI of the desired signal m_n

Specifically, in the uplink, the OMI is set at

$$\mathrm{m} = \begin{cases} m_n^{MIN} < m_n < m_n^{MAX} = m_{max}^{OPTIMUM} : \\ \quad \text{for desired signal (variable)} \\ m_{max}^{OPTIMUM} : \\ \quad \text{for undesired signals (constant).} \end{cases}$$

In the downlink, the OMI is set at

$m = m_n^{MIN} < m_n < m_n^{MAX}$ for all signals (variable)

Fig. 7-11 shows the calculation results of the OMI range of the desired signal that satisfies the requirements for an uplink and a downlink, where the requirements are $DUR_N(f_n,m) \geq 26.7$ for the uplink and both $DUR_N(f_n,m) \geq 26.7$ and CNR > 40 dB for the downlink. The maximum OMI m_n^{MAX} of the desired signal is given as the maximum OMI satisfying the above-mentioned requirements, and the minimum OMI m_n^{MIN} is given as the minimum OMI satisfying the requirements As Fig. 7-11 shows, m_n^{MAX} degrades with an increasing number of multiplex channels due to the increase of composite third-order distortion $CTB_N^{MOD}(f_n,m)$ and m_n^{MIN} is almost constant because, in the lower OMI range, the composite third-order distortion $CTB_N^{MOD}(f_n,m)$ is negligible and the dominant factor is the CNR.

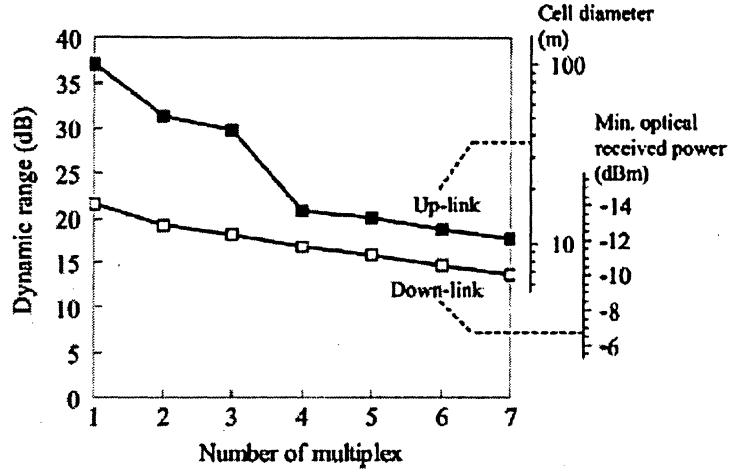

Fig. 7-12 Calculation results of dynamic range, cell diameter, and minimum optical received power.

Fig. 7-12 shows the dynamic range of the input signal versus the number of multiplex channels in both the uplink and downlink. As Fig.7-12 shows, by increasing the number of multiplex channels from one to seven, the dynamic range is degraded from 37 to 17.7 dB in the uplink, and from 21.6 to 13.8 dB in the downlink. The degradation in the uplink is much higher than that in the downlink. This is attributed to the fact that the amounts of composite third-order distortions generated by other channel signals are very different between the uplink and downlink.

From the results of the dynamic range above, it is evaluated several system parameters for a multichannel WLAN system. In the uplink, cell size, which is dominated by a dynamic range, is evaluated with free-space propagation model. In the downlink, all input signal levels to the LD are typically the same and constant—therefore, a wide dynamic range for the input

signal is not required. For this reason, an optical power budget is evaluated with the allocation of the dynamic range shown in Fig. 7-11.

The minimum optical received power Pr_{min}, which dominate the optical power budget is given by solving the following equation for ΔPr

$$\mathrm{CNR}\,(Pr_{\min}^{1ch} \Delta Pr) - \mathrm{CNR}\,(Pr_{\min}^{1ch}) = \Delta \mathrm{DR}$$

$$Pr_{min} = Pr_{\min}^{1ch} \Delta Pr \tag{18}$$

where $Pr_{\min}^{1ch} = 14$ dBm is the minimum optical received power for a single channel transmission, ΔPr is the relative optical received power of Pr_{min}, to $Pr_{\min}^{1ch}$, and ΔDR is the relative dynamic range of the multichannel to the single channel.

The evaluation results of cell size in the uplink and the minimum optical received power in the downlink are shown in the right vertical axis of Fig. 7-12. In the evaluation for the uplink, the cell diameter for a single-channel 11a signal are assumed as 100 m according to the free-space propagation loss under conditions of both the minimum received power of 65 dBm and the transmit power of 16 dBm [65]. From the result shown in Fig.7-12, the cell diameter in seven-channel transmission becomes 10.8 m.

In the evaluation of the downlink, It is assume that the OMI of all signals are set to m_n^{MAX} shown in Fig. 7-11, for maximizing the optical power budget, and that the minimum optical received power for a single-channel 11a signal is 14 dBm from the experimental results in Section III-A. From the result shown in Fig. 7-12, the minimum optical received power in seven-channel transmission is 10 dBm. Assuming that the optical sending power is 6 dBm, the optical power budget then becomes 16 dB where the optical transmission distance is 3 km, the optical fiber loss is 0.35 dB/km, the optical connector loss is 0.5 dB/piece X 2 pieces, and the 2^N-branch splitter loss is N X 3.5 dB, which shows that the downlink signal can be distributed to 16 RAUs.

From these results, the bidirectional optical transmissions of seven-channel WLAN signals can be realized by setting the OMI as the optimum condition. In the uplink, the maximum OMI of each signal should be limited at m_n^{MAX} shown in Fig. 7-11, which is 3.9%. In the downlink, the OMI of each signal should be set at m_n^{MAX} shown in Fig. 7-11, which is 12.1%.

8. CONCLUSION

In this project, we studied the performance of the OFDM-RoF system for the future wireless system design through the issues which may affect its performance. It has been observed that,

- Deliberate clipping may not be an efficient method to reduce the PAPR problem of OFDM because it gives a good ***PAPR*** only at the expense of some performance degradation. Clipping process introduces severe distortion that may result in irreducible bit error for the uncoded system and the use of channel coding may alleviate this degradation

- Clipping may not be a major source of issues regarding performance degradation, provided powerful channel coding is applied to the system with a constellation of relatively low order such as QPSK, the degradation in SNR may be small.

- SLM technique, and of the *PTS* approach, is more advantageous as it applies to an arbitrary number of subcarriers and to any size signal constellation. It is found that using 128 subcarriers and ***M=4,*** with values chosen from the set , it is shown that the 1% *PAP* (i.e., the *PAP* exceeds this value for less than 1% of the OFDM blocks) can be reduced **by** more than 2 dB .

- SLM and PTS are complex as SLM approach requires the use of ***M*** full-length (i,e., N-point) IFFTs at the transmitter. While the PTS approach uses a similar number of N-point IFFTs, if the transforms can take advantage of the fact that a large fraction of the input values are zero, the additional complexity can be kept to a minimum. Nevertheless, in the PTS approach, an optimization is required at the transmitter to best combine the partial transmit sequences. In its most direct form, this process requires the PAPR to be computed at every step of the optimization algorithm, necessitating numerous trials to achieve the optimum. It is found that about 2000 trials are required to get within 0.1 dB of the optimum .

- DUR is degraded with both the reduction of the relative signal level, which causes CNR degradation, and the increase of m_{max}, which causes CTB degradation.. For the OFDM-64QAM signal, the required DUR that realizes the PER = 0.1, is 26.7 dB. Therefore, the dynamic range is given by the OMI range satisfying that the DUR is more than 26.7 dB
- Dynamic Range = 20 log $[m_n^{MAX}/m_n^{MIN}]$ can be evaluated from DUR

- WLAN system with a cell diameter of 10 m, the bidirectional optical transmissions of seven-channel WLAN signals can be realized by properly setting the OMI, which is up to 3.9% in the uplink and 12.1% in the down link.

The key issues to be considered by designers of OFDM-ROF systems:

- According to the system requirements such as the channel coding, the number of subcarriers, transmitter complexity (e.g., the size of IDFT) and the maximum permissible PAPR for a given probability, the clipping ratio should be carefully designed.
- A clear relationship between the number of multiplex channels and system parameters for a multichannel WLAN system are required while focusing on the performance of the OFDM-ROF system.

This study can be further enhanced by analyzing the measurement values and distortion effects.

9. REFERENCES

[1] K. W. Richard, "UMTS overview", *IEE Electronics and Communication Engineering Journal*, Vol. 12, No. 3, June 2000, pp. 93 - 100

[2] Ermanno Berruto, Giovanni Colombo, Pantelis Monogioudis, Antonella Napolitano, Kyriacos Sabatakakis, "Architectural Aspects for the Evolution of Mobile Communications Toward UMTS", *IEEE Journal on Selected Areas in Communications*, Vol. 15, No. 8, October 1997, pp. 1477 - 1487

[3] Erik Dahlman, Björn Gudmundson, Mats Nilsson, Johan Sköld, "UMTS/IMT-2000 Based on Wideband CDMA", *IEEE Communications Magazine*, September 1998, pp. 70 - 80

[4] Fumiyuki Adachi, Mamoru Sawahasi, Hirohito Suda, "Wideband DS-CDMA for Next-Generation Mobile Communications Systems", *IEEE Communications Magazine*, September 1998, pp. 56 - 69

[5] Josef Huber, "3G Forum Leveraging Spectum Capacity In Accordance with 3G Deployment", *3G Forum* 17th-18th April 2001, Washington D. C., Online: http://www.umts-forum.org/ipapers/Leveraging_Spectrum_Capacity.pdf

[6] Douglas N. Knisely, Sarath Kumar, Subhasis Laha, Sanjiv Nanda, "Evolution of Wireless Data Services: IS-95 to cdma2000", *IEEE Communications Magazine*, October 1998, pp. 140 - 149

[7] "Third Generation Mobile Phone Licensing in Europe", *TIA on line*, Online: http://www.tiaonline.org/international/regional/nis/licensing.cfm, October 2000.

[8] "Auction of Third Generation Mobile Telecommunications Licences in the UK, Frequently Asked Questions", *Radiocommunications Agency of UK*, UMTS consultative group publication on may 1998 Online: http://www.spectrumauctions.gov.uk/documents/faq2.htm,

[9] "Spectrum Auctions", Radiocommunications Agency of UK, may 1998, UMTS consultative group online: http://www.spectrumauctions.gov.uk/auction/auction_index.htm

[10] S. Dehghan, D. Lister, R. Owen, P. Jones, "W-CDMA capacity and planning issues", *IEE Electronics and Communications Engineering Journal*, Vol. 12, No. 3, June 2000, pp. 101 - 118

[11] Sanjiv Nanda, Krishna Balachandran, and Sarath Kumar, "Adaptation Techniques in Wireless Packet Data Services", *IEEE Communications Magazine*, January 2000, pp. 54 - 64

[12] Terje Tjelta, Agne Nordbotten, Marco Annoni, Enrico Scarrone, Simone Bizzarri, Laurissa Tokarchuk, John Bigham, Chris Adams, Ken Craig, Manuel Dinis, "Future Broadband Radio Access Systems for Integrated Services with Flexible Resource Management", *IEEE Communications Magazine*, August 2001, pp. 56 - 63

[13] NTT DoCoMo Advertisement, "The Path to 4G Mobile", *IEEE Communications Magazine*, March 2000, pp. 38 - 41

[14] "Digital Video Broadcasting", ETSI, Online: http://www.etsi.org/broadcast/dvb.htm, October 2000

[15] "A Guideline for the use of DVB specifications and standards", DVB Blue Book A20, pp. 9, Online: www.dvb.org/news/pdf/dvb_cook.pdf

[16] ETSI EN 300 421, "Framing Structure, channel coding and modulation for 11/12 GHz satellite services", August 1997, pp. 6, Online: http://www.etsi.org

[17] Ulrich Reimers, "Digital Video Broadcasting", *IEEE Communications Magazine*, June 1998, pp. 104 - 110

[18] ETSI ETS 300 744, "Framing Structure, Channel Coding and Modulation for Digital Terrestrial Television", March 1997, online: http://www.etsi.org

[19] Louis Thibault, Minh Thien Le, "Performance Evaluation of COFDM for Digital Audio Broadcasting Part I: Parametric Study", *IEEE Transactions on Broadcasting*, Vol. 43, No.1, March 1997, pp. 64 – 75

[20] "Digital Audio Broadcasting - Overview and Summary of the DAB System", *World DAB Forum*, Online: http://www.worlddab.org/public_documents/eureka_brochure.pdf

[21] ETSI EN 300 401, "Radio Broadcasting Systems; Digital Audio Broadcasting (DAB) to mobile, portable and fixed receivers", May 2001, online: http://www.etsi.org

[22] Michel Mouly, Marie-Bernadette Pautet, "The GSM System for Mobile Communications", *M. Mouly et Marie-B. Pautet*, France, 1992, ISBN: 2-9507190-0- 7

[23] Siegmund Redl, Matthias Weber, Malcom Oliphant, "GSM and Personal Communications Handbook", *Artech House Publishers*, Norwood, 1998, ISBN: 0- 89006-957-3

[24] Telstra, "Flexi-Plans", Online: http://www.telstra.com.au/mobilenet/flexipln/dflex.cfm, November 2001

[25] Optus, "Rate Plans", Online: http://optusdirect.optus.com.au/shop/rateplans, November 2001

[26] William C. Y. Lee, "Overview of Cellular CDMA", *IEEE Transactions on Vehicular Technology*, Vol. 40, No. 2, May 1991, pp. 291 - 302

[27] Ryuji Kohno, Reuven Meidan and Laurence B. Milstein, "Spread Spectrum Access Methods for Wireless Communications", *IEEE Communications Magazine*, January 1995, pp. 58 - 67

[28] Yiyan Wu, William Y. Zou, "Orthogonal Frequency Division Multiplexing: A Multi- Carrier Modulation Scheme", *IEEE Transaction on Consumer Electronics*, Vol. 41, No. 3, August 1995, pp. 392 - 399

[29] William Y. Zou, Yiyan Wu, "COFDM: An Overview", *IEEE Transactions on Broadcasting*, Vol. 41, No. 1, March 1995, pp. 1 - 8

[30] R. R. Mosier and R. G. Clabaugh, "Kineplex, a bandwidth-efficient binary transmission system", AIEE Transactions, Vol. 76, January 1958, pp. 723 – 728

[31] Robert Chang, "Synthesis of Band-Limited Orthogonal Signals for Multichannel Data Transmission", The Bell System Technical Journal, December 1966, pp. 1775 -1796

[32] Robert Chang, "Orthogonal frequency division multiplexing", US. Patent 3,488445, filed November 14, 1966, issued January 6, 1970

[33] S. B. Weinstein, Paul M. Ebert, "Data Transmission by Frequency-Division Multiplexing Using the Discrete Fourier Transform", IEEE Transactions on Communication Technology, Vol. COM-19, No. 5, October 1971, pp. 628 - 634

[34] Carl Magnus Frodigh, Perols Leif Mikael Gudmundson, "Adaptive channel allocation in a frequency division multiplexed system", US. Patent 5,726,978, Filed: June 22, 1995, Issued: March 10, 1998

[35] M. Wahlqvist, C. Östberg, J. Beek, O. Edfors, P. Börjesson, "A Conceptual Study of OFDM-based Multiple Acess Schemes", Technical Report Tdoc 117/96, ETSI STC SMG2 meeting no 18, Helsinki, Finland, May 1996, Online: http://www.sm.luth.se/csee/sp/publications

[36] B. Crow, I. Widjaja, J. G. Kim, P. Sakai, "IEEE 802.11 Wireless Local Area Networks", *IEEE Communications Magazine*, pp 116 - 126, September 1997

[37] M. Johnsson, "HiperLAN/2 – The Broadband Radio Transmission Technology Operating in the 5 GHz Frequency Band", Online: http://www.hiperlan2.com/site/specific/specmain/specwh.htm, 1999

[38] ETSI, "Hiperlan/2-Technical Overview",
Online: http://www.etsi.org/technicalactiv/Hiperlan/hiperlan2tech.htm

[39] ETSI TS 101 475 V1.1.1, "Broadband Radio Access Networks (BRAN); HIPERLAN Type 2; Physical (PHY) layer", April 2000, online: http://www.etsi.org

[40] "Part 11: Wireless LAN Medium Access Control (MAC) and Physical Layer (PHY) specifications: High-speed Physical Layer in the 5 GHZ Band", *IEEE Std 802.11a-1999*, September 1999

[41] Martin S. Roden, "Analog and Digital Communication Systems", *Prentice-Hall International, Inc*, 4th Edition, 1996, ISBN: 0-13-399965-3

[42] B. P. Lathi, "Modern Digital and Analog Communication Systems", *CBS College Publishing*, 1983, ISBN: 0-03-058969-X

[43] Yoshihiko Akaiwa, "Introduction to Digital Mobile Communication", *John Wiley & Sons, Inc*, 1997, ISBN: 0-471-17545-5

[44] A. J. Seeds, "Wireless access over optical fiber: From cellular radio to broadband; from UHF to millimeter-waves," in *Proc. LEOS*, 2002, pp. 471–472.

[45] E. I. Ackerman and C. H. Cox, "RF fiber-optic link performance," *IEEE Micro*, vol. 2, pp. 50–58, Dec. 2001. NIIHO *et al.*: TRANSMISSION PERFORMANCE OF MULTICHANNEL WLAN BASED ON RoF TECHNIQUES 989

[46] C. Cox, E. Ackerman, R. Helkey, and G. E. Betts, "Techniques and performance of intensity-modulation direct-detection analogue optical links," *IEEE Trans. Microwave Theory Tech.*, vol. 45, no. 8, pp. 1375–1383, Aug. 1997.

[47] Y. Ebine, "Development of fiber-radio system for cellular mobile communications," in *Proc. Microw. Phonton.* 1999, pp. 249–252.

[48] H. Sasai, H. Yamamoto, K. Utsumi, and K. Fujito, "High performance fiber-optic sub-carrier multiplexing transmission using unisolated Fabry–Perot lasers for mobile radio system," in *OSA TOPS*, vol. 12, 1997, pp. 318–323.

[49] D. Wake, "Trends and prospects for radio over fiber picocells," in *Proc. Microw. Photon.* 2002, pp. 21–24.

[50] Y. Ito and Y. Ebine, "Radio on fiber system for triple band transmission in cellular mobile communication," in *Proc. Microw. Photon.* 2000, pp. 35–38.

[51] *Wireless LAN Medium Access Control (MAC) and Physical Layer (PHY) Specifications: High-Speed Physical Layer in the 5 GHz Band*, IEEE Standard 802.11a-1999, Part 11, 1999.

[52] *Wireless LAN Medium Access Control (MAC) and Physical Layer (PHY) Specifications: Higher-Speed Physical Layer Extension in the 2.4 GHz Band"*, IEEE Standard 802.11b-1999, Part 11, 1999.

[53] H. Sasai, T. Niiho, K. Tanaka, K. Utsumi, and S. Morikura, "Radio-over- fiber transmission performance of OFDM signal for dual-band wireless LAN systems," in *Proc. Microw. Photon.*, 2003, pp. 139–142.

[54] K. Utsumi, H. Sasai, T. Niiho, M. Nakaso, and H. Yamamoto, "Multiband wireless LAN distributed antenna system using radio-over-fiber," in *Proc. Microw. Photon.*, 2003, pp. 363–366.

[55] T. Niiho, H. Sasai, K. Masuda, and S. Morikura, "Radio-on-fiber link using direct modulation in 5 GHz band," in *Proc. Microw. Photon.*, 2002, pp. 25–28.

[56] *Broadband Mobile Access Communication System (CSMA)*, ARIB Standard T71, 2003.

[57] T. Niiho, H. Sasai, K. Tanaka, K. Utsumi, and S. Morikura, "Bi-directional radio-over-fiber transmission of 5-GHzOFDM Signal for wireless LAN systems," in *Proc. ECOC–IOOC*, 2003, pp. 782–783.

[58] R. W. Bäuml, R. F. H. Fischer, and J. B. Huber, "Reducing the peak-toaverage power ratio of multicarrier modulation by selected mapping,"*Electron. Lett.*, vol. 32, pp. 2056–2057, Oct. 1996.

[59] D. J. G. Mestdagh and P. M. P. Spruyt, "A method to reduce the probability of clipping in DMT-based transceivers," *IEEE Trans. Commun.*, vol. 44, pp. 1234–1238, Oct. 1996.

[60] H. Ochiai and H. Imai, "Performance of the deliberate clipping with adaptive symbol selection for strictly band-limited OFDM systems," *IEEE J. Select. Areas Commun.*, vol. 18, pp. 2270–2277, Nov. 2000.

[61] S. H. Müller, R. W. Bäuml, R. F. H. Fischer, and J. B. Huber, "OFDM with reduced peak-to-average power ratio by multiple signal representation," *Ann. Télécommun.*, vol. 52, pp. 58–67, Feb. 1997.

[62] M. Friese, "OFDM signals with low crest-factor," in *Proc. IEEE GLOBECOM '97*, vol. 1, New York, NY, Nov. 1997, pp. 290–294.

[63] J. Tellado and J. Cioffi, "Peak power reduction for multicarrier transmission," in *Proc. IEEE CTMC, GLOBECOM '98*, Sydney, Australia, Nov. 1998, pp. 219–224.

[64] R. D. J. van Nee, "OFDM codes for peak-to-average power reduction and error correction," in *Proc. IEEE GLOBECOM '96*, London, U.K, Nov. 1996, pp. 740–744.

[65] J. A. Davis and J. Jedwab, "Peak-to-mean power control in OFDM, Golay complementary sequences and Reed-Muller codes," *IEEE Trans. Inform. Theory*, vol. 45, pp. 2397–2417, Nov. 1999.

[66] H. Ochiai and H. Imai, "Block coding scheme based on complementary sequences for multicarrier signals," *IEICE Trans. Fundamentals*, vol. E80-A, pp. 2136–2143, Nov. 1997.

[67] R. O'Neill and L. B. Lopes, "Envelope variations and spectral splatter in clipped multicarrier signals," in *Proc. PIMRC '95*, vol. 1, Toronto, Canada, Sept. 1995, pp. 71–75.

[68] X. Li and L. J. Cimini Jr, "Effects of clipping and filtering on the performance of OFDM," in *Proc. VTC '97*, Phoenix, AZ, May 1997, pp. 1634–1638.

[69] D. Wulich and L. Goldfeld, "Reduction of peak factor in orthogonal multicarrier modulation by amplitude limiting and coding," *IEEE Trans. Commun.*, vol. 47, pp. 18–21, January 1999.

[70] D. Kim and G. L. Stüber, "Clipping noise mitigation for OFDM by decision- aided reconstruction," *IEEE Commun. Lett.*, vol. 3, pp. 4–6, Jan. 1999.

[71] R. Dinis and A. Gusmão, "On the performance evaluation of OFDM transmission using clipping techniques," in *Proc. IEEE VTC '99 Fall*, Amsterdam, The Netherlands, Sept. 1999, pp. 2923–2928.

[72] C. Tellambura, "Use of pseudo random-sequences for OFDM peak-to-average power ratio reduction," *Electron. Lett.*, vol. 33, pp. 1300–1301, July 1997.

[73] R. Price, "A useful theorem for nonlinear devices having gaussian inputs," *IRE Trans. Inform. Theory*, vol. IT-4, pp. 69–72, June 1958.

[74] R. Deutsch, *Nonlinear Transformations of Random Processes*. Englewood Cliffs, NJ: Prentice-Hall, 1962. [18] G. Santella and F. Mazzenga, "A hybrid analytical-simulation procedure for performance evaluation in M-QAM-OFDM schemes in presence of nonlinear distortions," *IEEE Trans. Veh. Technol.*, vol. 47, pp. 142–151, Feb. 1998.

[75] M. Friese, "On the degradation of OFDM-signals due to peak-clipping in optimally predistorted power amplifier," in *Proc. IEEE GLOBECOM '98*, Sydney, Australia, Nov. 1998, pp. 939–944.

[76] E. Costa, M. Midrio, and S. Pupolin, "Impact of amplifier nonlinearities on OFDMtransmission system performance," *IEEE Commun. Lett.*, vol. 3, pp. 37–39, Feb. 1999.

[77] D. Dardari, V. Tralli, and A. Vaccari, "A theoretical characterization of nonlinear distortion effects in OFDM systems," *IEEE Trans. Commun.*, vol. 48, pp. 1755–1764, Oct. 2000.

[78] P. Banelli and S. Cacopardi, "Theoretical analysis and performance of OFDM signals in nonlinear AWGN channels," *IEEE Trans. Commun.*, vol. 48, pp. 430–441, Mar. 2000.

[79] C. Berrou and A. Glavieux, "Near optimum error correcting coding and decoding: Turbo-codes," *IEEE Trans. Commun.*, vol. 44, pp. 1261–1271, Oct. 1996.

[80] G. L. Stüber, *Principles of Mobile Communications*. Norwell, MA: Kluwer, 1996.

[81] H. E. Rowe, "Memoryless nonlinearities with gaussian inputs: Elementary results," *Bell Syst. Tech. J.*, vol. 61, pp. 1519–1525, Sept. 1982.

[82] J. G. Proakis, *Digital Communications*, 3rd ed. New York: McGraw- Hill, 1995.

[83] S. G. Wilson, *Digital Modulation and Coding*. Englewood Cliffs, NJ: Prentice-Hall, 1996.

[84] H. Ochiai, "Analysis and Reduction of Peak-to-Average Power Ratio in OFDM Systems," Ph.D., Univ. of Tokyo, 2001.

[85] H. Ochiai and H. Imai, "On the distribution of the peak-to-average power ratio in OFDM signals," *IEEE Trans. Commun.*, vol. 49, pp. 282–289, Feb. 2001.

[86] , "On clipping for peak power reduction of OFDM signals," in *Proc. IEEE GLOBECOM '00*, vol. 2, San Francisco, CA, Nov. 2000, pp. 731–735.

[87] J. Minkoff, "The role of AM-to-PM conversion in memoryless nonlinear systems," *IEEE Trans. Commun.*, vol. COM-33, pp. 139–144, Feb. 1985.

[88] W. Feller, *An Introduction to Probability Theory and its Applications*, 2nd ed. New York: Wiley, 1957, vol. 1.

[89] R. G. Gallager, *Information Theory and Reliable Communication*. New York: Wiley, 1968.

[90 R. W. Bauml, R. F. H. Fischer, and J. B. Huber, "Reducing the Peak-to-Average Power Ratio of MulticarrierModulation by Selective Mapping," ***Elec. Letts.,*** Vol. 32, No.

[91] S. H. Muller and J. B. Huber, "OFDM with Reduced Peak-to-Average Power Ratio by Optimum Combination of Partial Transmit Sequences,' ***Elec. Letts.,*** Vol. 33, No. 5, Feb.1997

[92]S.Wen and T.K.Lin "Ultralong lightwaves systems with incomplete dispersion compensations,"journal of light wave technology vol .19 April 2000

[93]G.P Agarwal.Nonlinear fiber optics and application of nonlinear fiber optics, Beijing publishing house of electronics industry 2002; 33-35

[94] G. Ungerboeck, "Channel coding with multilevel/phase signals," *IEEE Trans. Inform. Theory*, vol. IT-28, pp. 55–67, Jan. 1982.

[95] L.Rao, X.Sun, W.Li and D.Huang, 'OFDM-ROF System and performance Analysis of Signal Transmission' optoelectronics, 2006 optics valley of china international symposium on Nov. 2006 pp67-70, 1-4244-0816-4/06IEEE 2006

[96] H.Ochiai and H.Imai "Performance Analysis of Deliberately clipped OFDM signals, IEEE transactions on communications volume 50, no.1 january2002

[97] T Niiho,M.Nakaso,K.Masuda,H.Sasai,K.Utsumi and M.fuse, "Transmission Performance of multichannel wireless system based on Radio-over-Fiber Techniques. IEEE transactions on microwave theory and techniques, vol.54, no.2, February 2002

[98] L. Cimini, J. Chuang, N. Sollenberger, "Advanced Cellular Internet Service (ACIS)", *IEEE Communications Magazine*, Oct. 1998, pp. 150 – 159

[99 A. E. Jones, T. A. Wilkinson, and *S.* K. Barton, "Block Coding Scheme for Reduction of Peak to Mean Envelope Power Ratio of Multicarrier Transmission Scheme," ***Elec. Letts.,*** Vol. 30, No. 25, Dec. 1994, pp. 2098-2099.

[100] R. D. J. van Nee, "OFDM Codes for Peak-to-Average Power Reduction and Error Correction," ***Proc.*** Of ***Globecom '96,*** pp. 740-744.

[101] P. Van Eetvelt, G. Wade, and M. Tomlinson, "Peak to Average Power Reduction for OFDM Schemes by Selective Scrambling," ***Elec. Letts.,*** Vol. 32, No. 21, Oct. 1996, pp.